Influence of mannitol concentration on the physicochemical, mechanical and pharmaceutical properties of lyophilised mannitol

Title: Influence of mannitol concentration on the physicochemical, mechanical and pharmaceutical properties of lyophilised mannitol

Author: Waseem Kaialy Usman Khan Shadan Mawlud

PII: S0378-5173(16)30441-0
DOI: http://dx.doi.org/doi:10.1016/j.ijpharm.2016.05.052
Reference: IJP 15791

To appear in: *International Journal of Pharmaceutics*

Received date: 30-3-2016
Revised date: 23-5-2016
Accepted date: 26-5-2016

Please cite this article as: Kaialy, Waseem, Khan, Usman, Mawlud, Shadan, Influence of mannitol concentration on the physicochemical, mechanical and pharmaceutical properties of lyophilised mannitol.International Journal of Pharmaceutics http://dx.doi.org/10.1016/j.ijpharm.2016.05.052

Influence of mannitol concentration on the physicochemical, mechanical and pharmaceutical properties of lyophilised mannitol

Waseem Kaialy*, Usman Khan, Shadan Mawlud

School of Pharmacy, Faculty of Science and Engineering, University of Wolverhampton, Wolverhampton, WV1 1LY, UK

*Corresponding author

Waseem Kaialy, Tel: +441902321139, E-mail: w.kaialy@wlv.ac.uk

Graphical Abstract

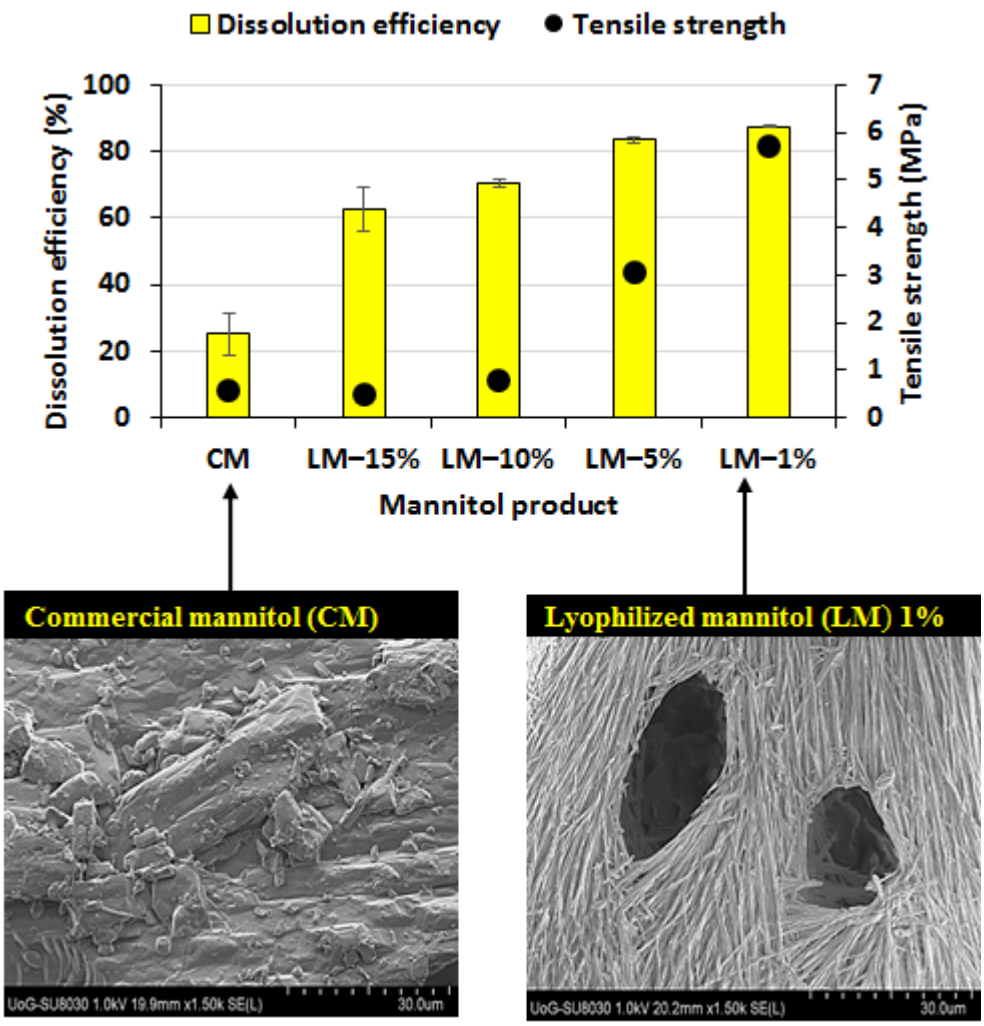

Abstract

Mannitol is a pharmaceutical excipient that is receiving increased popularity in solid dosage forms. The aim of this study was to provide comparative evaluation on the effect of mannitol concentration on the physicochemical, mechanical, and pharmaceutical properties of lyophilised mannitol. The results showed that the physicochemical, mechanical and pharmaceutical properties of lyophilised mannitol powders are strong functions of mannitol concentration. By decreasing mannitol concentration, the true density, bulk density, cohesivity, flowability, netcharge-to-mass ratio, and relative degree of crystallinity of LM were decreased, whereas the breakability, size distribution, and size homogeneity of lyophilised mannitol particles were increased. The mechanical properties of lyophilised mannitol tablets improved with decreasing mannitol concentration. The use of lyophilised mannitol has profoundly improved the dissolution rate of indomethacin from tablets in comparison to commercial mannitol. This improvement exhibited an increasing trend with decreasing mannitol concentration. In conclusion, mannitols lyophilised from lower concentrations are more desirable in tableting than mannitols from higher concentrations due to their better mechanical and dissolution properties.

Abbreviations

ΔH_0, Endothermic enthalpy of CM melting; ΔH_s, Endothermic enthalpy of LM melting; ANOVA, One-way analysis of variance; API, Active pharmaceutical ingredient; c.opt, Optimal concentration; CI, Carr's index; CM, Commercial mannitol; C_{man}, Concentration of mannitol; $d_{10\%}$, particle size at 10% volume distribution; $d_{50\%}$, particle size at 50% volume distribution; $d_{90\%}$, particle size at 90% volume distribution; D_b, Bulk density, DE, Dissolution efficiency; DSC, Differential scanning calorimeter; D_t, tap density; EB, Ease of breakage; Eq, Equation; FT–IR, Fourier transform infrared; GI, Gastro intestinal; HSD, Honestly Significant Difference; *I*, Relative intensity; $I_{amorphous}$, the input to the intensity from the amorphous region; $I_{crystalline}$, the input to the intensity from the crystalline region; LM, Lyophilised mannitol; MDR, Mean dissolution rate; MDT, Mean dissolution time; *P*, Statistical probability; PXRD, Powder X–ray diffraction; Q_{10min}, The mean percentage of drug dissolved in the first 10 min; Q_{30min}, The mean percentage of drug dissolved in the first 30 min; Q_{4min}, The mean percentage of drug dissolved in the first 4 min; Q_{50min}; The mean percentage of drug dissolved in the first 50 min; RDB, Relative degree of breakage; SD, Standard deviation; SEM, Scanning electron microscopy; SM, Supplementary material; T_g, Glass transition temperature; TS, tensile strength.

Keywords

Dissolution; Freeze-drying (lyophilisation); Indomethacin; Mannitol; Molecular, micromeritic and bulk properties; Tablets.

Chemical compounds studied in this article

D-Mannitol (PubChem CID: 6251); Indomethacin (PubChem CID: 3715)

1. Introduction

Industrially, the ordinary method to produce pharmaceutical compounds in the micrometer size range is the 'top-down' size reduction by milling (Kaialy and Al Shafiee, 2015). However, despite its popularity, milling has several disadvantages (Parrott, 1990). For example, milling offers low opportunity to produce particles with controlled characteristics such as size, shape and surface properties (Snow et al., 1984). Jet-milled particles usually exhibit broad size distributions, irregular shapes (Rasenack and Müller, 2004), and high levels of electrostatic charges, resulting in increased interparticle cohesive forces and potentially leading to poor product performance (Brodka-Pfeiffer et al., 2003; Kaialy, 2016). Moreover, jet-milling is incompatible with thermally sensitive materials and may raise safety worries due to dust exposure during processing (Tong and Chow, 2006).

Particle engineering techniques have been a subject to continuous improvement (Blagden et al., 2007). In contrast to jet-milling, particles with precisely engineered physical properties were, for instance, engineered using antisolvent crystallization (Kaialy et al., 2014, 2010), batch cooling crystallization (Kaialy et al., 2012), spray drying (Vehring, 2008), spray-freeze drying (Rogers et al., 2003), etc. Freeze-drying (lyophilisation) is a technical procedure that involves the removal of frozen water by sublimation. Lyophilised formulations commonly contain mannitol ($C_6H_{14}O_6$) as a bulking agent to increase the drug volume and thus preventing the 'blow-out' phenomenon that may occur in the case of a solution having a content of solute less than 1*%*, *w*/*v* (Franks and Auffret, 2008). The relatively high melting temperature of the mannitol/ice eutectic mixture (~ −1.5 °C) promotes efficient drying and physical stability of lyophilised mannitol (LM) solids (Kim et al., 1998). Mannitol can be lyophilised to produce a crystalline product, with the only precaution to maintain the temperature below that of incipient melting (Barresi et al., 2009). Therefore, the lyophilisation of 10*% w*/*w* solutions resulted in crystalline and amorphous materials of mannitol and sucrose respectively (Franks and Aufrett, 2007). Although amorphous mannitol can serve as a stabiliser for the active pharmaceutical ingredient (API) (Izutsu et al., 1994), the difficultly to maintain mannitol in the amorphous state during lyophilisation makes mannitol a poor choice as stabiliser (Pikal, 2002). However, the crystallisation of mannitol in frozen solutions during lyophilisation was inhibited by using phosphate buffer salts (Izutsu et al., 1994), polyvinylpyrrolidone (Cavatur et al., 2002) and NaCl (Telang et al., 2003).

During lyophilisation, mannitol was shown to crystallise as three common stable anhydrous polymorphic forms (i.e. *α*, *β* and *δ*) (Bauer et al., 2000; Berman et al., 1968; Botez et al., 2003; Burger et al., 2000; Kim et al., 1968) or as mannitol hemihydrate (Cavatur and Suryanarayanan, 1998; Cavatur et al., 2002; De Beer et al., 2007; Nunes et al., 2004; Romero-Torres et al., 2007; Yu et al., 1999). The polymorphic form of lyophilised mannitol was shown to have an effect in the stability of the lyophilised product during its storage (Cao et al., 2006; De Beer et al., 2009, 2007; Pisano et al., 2013). For example, the presence of hemihydrate mannitol in a lyophilised product could increase the rate of degradation, because hemihydrate mannitol is transformed during storage into anhydrous crystalline *δ*–mannitol by releasing its hydrate water within the amorphous phase containing the active pharmaceutical ingredient (Ahlneck and Zografi, 1990; Nunes et al., 2004). (Pisano et al., 2013) showed that a high content of mannitol in formulations containing mannitol and sucrose could better protect the enzyme molecules (acid phosphatase) from the dehydration stresses of lyophilization. Several studies showed the selection of the freezing method (Oddone et al., 2016) and the process conditions (Gan et al., 2004; Rene et al., 1993; Velardi and Barresi, 2008) as important parameters to be considered during cycle development. For example, (Kim et al., 1998) showed that a mixture of *α*– and *β*–mannitol was produced by slow freezing of 10% (*w*/*v*) mannitol, whereas fast freezing of 10% (*w*/*v*) and 5% (*w*/*v*) mannitol produced *δ*– and *β*–mannitol respectively. (Barresi et al., 2009) showed the temperature at which primary drying is carried out to affect the bulk density, rehydratability and residual moisture content of the lyophilised product. Higher rehydration rates were observed for products lyophilised at lower temperatures and lower initial concentrations. (Yu et al., 1999) showed the secondary drying conditions during freeze-drying as important parameters for the removal of the mannitol hemihydrate form. (Cannon and Trappler, 1999) showed slow cooling rates to promote the formation of *α*–mannitol. The use of surfactants, e.g. pluronic F68 (Hottot et al., 2008) and polysorbate (Haikala and Eerola, 1997), was shown to induce the formation of *δ*–mannitol phase and inhibit mannitol crystallisation.

Mannitol is an attractive pharmaceutical excipient that is becoming more and more popular in solid dosage forms (Ohrem et al., 2014). Mannitol shows the lowest hygroscopicity among the frequently used excipients as filler/binder and hence it can be utilized for moisture-sensitive drugs. Furthermore, mannitol does not increase the levels of blood glucose to such an extent as lactose (Geil, 1996) and thus it is especially suitable for pharmaceutical formulations

that are used for diabetics (Zumbe et al., 2001). There is currently a strong driving force to use mannitol as an alternative excipient to lactose in pharmaceutical formulations (Eadala et al., 2009). This is because lactose exhibits unpredictable physicochemical properties during pharmaceutical production processes such as milling (Steckel et al., 2006) and crystallization (Zeng et al., 2000). Although lactose monohydrate is the most commonly used filler in tablet manufacture, lactose particles are required to have small size distributions to show good compactibility, leading to poor flow properties (Vromans, 1987). Additionally, lactose has a degree of security as inert excipient due to its incompatibility with compounds that have primary amine moieties (e.g. budesonide and formoterol), since Maillard-type condensation reaction is likely to occur (Bharate et al., 2010). Furthermore, although the side effects of lactose intolerance will sometimes not be observed in a patient using the small amounts of lactose present in tablets, the NOCEBO-effect should not be ignored. Therefore, lactose-free formulations may be needed for lactose-intolerant patients (Picksak and Stichtenoth, 2009). Moreover, lactose is produced from bovine milk or with bovine-driven additives, thus it carries a potential risk of transmissible spongiform encephalopathy (EMA, 2002). Mannitol is valuable in the production of tablets due to its excellent mechanical compressing properties, physical and chemical stability (Ohrem et al., 2014). Toxicity studies indicated that mannitol did not cause any considerable adverse effects (Lawson, 2000).

This study contributes to the development of mannitol as a potential excipient of the first choice. The purpose was address the theory that the physicochemical, mechanical and pharmaceutical properties of lyophilised mannitol (LM) powders are strongly dependent on the concentration of mannitol solution subjected to lyophilisation as one variable.

2. Materials and methods

2.1.Materials

Commercial mannitol (CM) was purchased from Fisher Scientific, UK. Indomethacin was purchased from Sigma-Aldrich, USA. Dissolution buffers were prepared according to the USP using potassium phosphate monobasic-white crystals (Fisher BioReagents, UK) and sodium hydroxide (Fisher Scientific, UK) for pH 7.2.

2.2.Preparation of lyophilised mannitols

A series of mannitol solutions with concentrations of 15%, 10%, 5% and 1% (*w*/*v*) were prepared by separately dissolving 15 g, 10 g, 5 g and 1 g of mannitol in distilled water such that the final volume of each solution is 100 mL. Each solution was then filtered (<0.45 µm, cellulose filter paper), filled into 250 mL round-bottomed flasks (50 mL per flask), and consequently lyophilised using a similar protocol as follows. The flasks were kept in a freezer (−80 ºC) for 12 h. The flasks containing the frozen mannitol solutions were quickly placed on the shelves of a Christ Beta 1-8 LD Freeze Dryer (Martin Christ Gefriertrocknungsanlagen GmbH, Osterode am Harz, Germany) using manifolds. The primary drying was performed at a shelf temperature of −27 ºC, vacuum pressure of 0.518 mbar and a safety pressure of 0.700 mbar, whereas the final drying was performed at a shelf temperature of −35 ºC, vacuum pressure of 0.224 mbar and a safety pressure of 0.380 mbar. For safety reasons (especially for mannitols lyophilised from the lowest concentrations, i.e. 1% *w*/*v*), the primary drying was carried out at a fixed low temperature for all samples in order to avoid collapse or 'blow-out' and to promote faster rehydratability of the LM products (Barresi et al., 2009; Franks and Auffret, 2008; Pikal-Cleland et al., 2000). The LMs were collected after 48 h. Fluffy LM powders were obtained with yields above 99% (*w*/*w*). The LM powders were sieved through a 0.50 mm sieve (Retsch® Gmbh Test Sieve, Germany), and stored in sealed glass vials in laboratory conditions (22 ºC, 50% RH) until used. The preparations were performed at least in triplicate using an identical protocol to ensure reproducibility.

2.3.Helium pycnometry

An electronic balance was used to measure the mass of a sample of each LM with an accuracy of 10^{-4} g. The true volume of each mannitol sample (the volume apart from both open and closed pores) was determined using an Ultrapycnometer 1000 (Quantachrom, USA) under helium gas at an input pressure of 20 psi. A multi-run system was used with a standard deviation of 0.005% and an equilibrium time of 1 min. The true volume was calibrated with a calibration sphere (Quantachrome Corp.) and calculated from the change in pressure when a specific volume of helium is purged into the chamber. The mean of nine determinations was recorded for each sample.

2.4.Bulk properties

An accurately weighed amount of each powder was gently poured into a 10–mL glass measuring cylinder using a glass funnel. The bulk volume was recorded and then the cylinder was tapped (Tapped Density Tester, Copley Scientific, UK) under laboratory conditions (22 °C, 50% = RH) for 500 taps (which was shown to produce the maximum reduction of powder bed for all samples). The volume was recorded after every 50 taps. Bulk density (or apparent density, D_b), tap density (or drop density, D_t), porosity (Eq. 1) and Carr's index (CI, Eq. 2) of each powder were calculated as follows.

$$\text{Porosity} = \left(1 - \frac{D_t}{D_{true}}\right) \times 100 \quad (1)$$

$$\text{CI} = \left(\frac{D_t - D_b}{D_t}\right) \times 100 \quad (2).$$

The packability was determined from the tapped density according to Kawakita and Ludde equation (Eq. 3) (Kawakita and Lüdde, 1971) as follows.

$$\frac{n}{C} = \frac{1}{ab} + \frac{n}{a} \quad (3),$$

$$C = \frac{V_0 - V_n}{V_0} \quad (4),$$

where n is the tap number, C donates the volume reduction (Eq. 4), and V_0 and V_n are the powder bed volumes at the initial and n^{th} tapped state respectively. The plot of n/C versus n is linear. Through the modified Kawakita and Ludde equation (Kawakita and Lüdde, 1971), the compactability ($1/a$) can be obtained from the slope a, and the cohesivity $1/b$ is obtained from the intercept $1/ab$ of the plot. The compactibility ($1/a$) defines the degree of volume reduction and the cohesivity ($1/b$) is a constant related to cohesion. Five different samples were analysed for each mannitol product.

2.5.Laser diffraction

Volume-weighted particle size analysis was conducted using a Sympatec (Clausthal–Zellerfeld, Germany) particle size analyser. To get primary particle size data (i.e. total dispersion), HELOS (H1730) & Cuvette (50 mL) system equipped with MS7 magnetically stirred cell and R5 lens (measuring range: from 0.5/4.5 µm to 875.0 µm) were used. The dispersion system was acetone

saturated with mannitol, sonicated for 30 min, stirred overnight and then filtered (< 0.45 μm, cellulose filter paper). A (100 to 200) mg sample of each product was dispersed in the dispersion system filled in a cuvette. A test reference (i.e. background measurement) was performed with the HELOS sensor using WINDOX 4.0 software followed by a standard measurement. The particle size measurements were carried out under stirring dispersion conditions (2000 rpm). Particle size at 10% ($d_{10\%}$), 50% (median diameter, $d_{50\%}$) and 90% ($d_{90\%}$) diameter based on volume distribution were calculated using the WINDOX 5 software (V 5.9.1.0). The optimal concentration (c.opt) ranged between 15 and 50% and the timebase was 1 ms. The width of the distribution relative to $d_{50\%}$ was measured by calculating the span of the volume distribution (Eq. 5).

$$\textbf{Span} = \frac{d_{90\%} - d_{10\%}}{d_{50\%}} \qquad \textbf{(5)}.$$

Ten samples were measured for each mannitol product.

For each sample, 20 sonications were applied consequently and the particle size data were recorded immediately to establish the influence of sonication time on the size of LM particles. Each sonication was for 10 s and the time between sonication and another was 1 min (the total effective sonication time applied for each sample was 200 s). To observe the relaxation of the effects of sonication on LM particles, the particle size of each sonicated (200 s) LM sample was monitored after 1 min, 15 min, 1 h and 3 h at the end of sonication. The particle size data were analysed by the following method to extract a 'relative degree of breakage' (RDB) parameter as follows (Eq. 6).

$$\textbf{RDB} = \frac{d50\%_{t=0}}{d50\%_{t=200}} \qquad \textbf{(6)}.$$

The particle size (expressed as the median diameter) at each ultrasonication time ($d50\%_{t=0}$) was expressed as a proportion to the smallest achievable particle size ($d50\%_{t=200}$). The RDB was thus as a measure of the relative degree of particle breakage at any particular time. The RDB data were empirically modelled using the modified Michaelis–Menten equation linearised using the Hanes–Woolf method (Eq. 7).

$$\frac{\mathbf{t}}{\mathbf{RDB}} = \frac{\mathbf{1}}{\mathbf{EB}} . \mathbf{t} + \frac{\mathbf{EB_{50\%}}}{\mathbf{EB}} \qquad \textbf{(7)},$$

where EB is the 'ease of breakage' which represents the maximum RDB calculated using the slope of the fitted regression line (SM–1). The $EB_{50\%}$ represents the 50% RDB calculated from the intercept and slope of the regression line.

2.6.Scanning electron microscopy

A representative specimen of each LM sample was gently mounted on an aluminium stub covered with carbon. To increase the electric conductivity on the surface of the samples, a sputter coater (Edwards S 150B Sputter Coater, Edwards High Vacuum, West Sussex, UK) was used to coat the samples with chromium (12 nm layer thickness) in an argon atmosphere before observation. Electron micrographs of LM samples were obtained using a scanning electron microscope (SEM, HITACHI SU 8030, Japan) operating at an acceleration voltage of 1 kV and probe current of 10 μA. Various magnifications (×130, ×500 and ×1500) were used to analyse the size, shape and surface texture of different LMs.

2.7.Electrostatic charging

The electrostatic charging properties of powders were analysed using a recent novel approach developed in the Wolfson Centre (University of Greenwich, UK) as described in (Hussain et al., 2013). The experimental apparatus used to investigate the electrostatic charging of powders consists of a single non-contact electrostatic inductive sensor (i.e. a probe), a charge amplifier unit, a national instrument data acquisition equipment, and a personal computer for data recording and processing. This method allows the detection and measurement of charge distribution on the charge sign basis in a population of particles (Hussain et al., 2016). A sample of each powder was fed in the cylindrical sensor with the help of a vibratory feeder and conveyed toward the sensor by gravity in a vertical direction. Special care was taken by considering the adhesion properties of the particles with the wall of the sensor. After each experiment, the inner tube was replaced to remove any deposits, impurities or surface charge that may have been present on the surface from a previous test. A fresh sample was used for each test experiment. Each sample was analysed six times in a temperature and humidity controlled laboratory (22 °C, RH = 50%). The positive charge is the sum of all positive charges whereas the negative charge is the sum of all negative charges. The netcharge is the sum of positive and negative charges. The charge-to-mass ratio

(CMR) was defined as the charge (negative charge for N–CMR, positive charge for P–CMR and netcharge for net–CMR) per unit mass, in nC/g.

2.8.Differential scanning calorimetry

A differential scanning calorimeter (DSC822^e, Mettler Toledo, Linseis, Germany) was conducted to characterise the solid-state of LMs. An accurately weighed sample of each LM product was placed in crimped aluminium 40–µL pans, and then heated from 25 °C to 200 ºC at a heating ramp rate of 30 ºC/min under a nitrogen gas atmosphere (50 L/min). An empty aluminium pan was used as the reference. Temperature and enthalpy readings were calibrated using pure indium heated at 30 ºC/min. The transition areas were automatically normalized for the weight of each sample using the STARe SW 11.00 software (Mettler, Switzerland). The % relative degree of crystallinity (RDC_{DSC}) of each LM product was estimated from the ratio of the endothermic enthalpy of LM melting (ΔH_s) to the calorimetric enthalpy of the melt of the reference crystalline mannitol (D-Mannitol, Fisher Scientific, UK) (ΔH_0) (Eq. 8).

$$\mathbf{RDC_{DSC} = 100 \times \left(\frac{\Delta H_s}{\Delta H_o}\right)} \qquad \mathbf{(8)}.$$

Four different samples were analysed for each mannitol product.

2.9.Fourier transform infrared spectroscopy

To investigate whether mannitol was chemically altered during the freeze-drying process, the molecular structure of all LMs was analysed using an Alpha Platinum−ATR FT−IR spectrometer (BRUKER, USA). A few milligrams of each powder were placed into the middle of the sample stage, and then compressed by twisting the top of the arm of sample stage. The samples were scanned between 650 cm^{-1} and 4,000 cm^{-1} with a 1 cm^{-1} resolution. The spectrum produced for each sample was a consequence of averaging 15 scans.

2.10. Powder X–ray diffraction

Powder X–ray diffraction (PXRD) structural patterns of mannitols were collected using a Panalytical Empyrean diffractometer (PANanalyical, Almelo, The Netherlands) powder diffractometer with Cu Kα radiation (1.54056 Å) operated at laboratory conditions (22 ºC, RH = 50%). Each sample was placed in a sample holder, surface-smoothed with a glass slide, and

scanned between 5º and 40º in 2Θ with a step-by-step increase of 0.01º 2Θ/1 s. The sample stage was spun at 30 rpm. The instrument was calibrated using a silicon standard.

The identification of the different polymorphs of mannitol was achieved from the 2θ peaks at the following angle positions: *α*–polymorph at 13.6° and 17.2°, *β*–polymorph at 14.6° and 23.4°, and *δ*–polymorph at 9.7° (Walter-Levy, 1968). Quantitative analysis of mannitol crystal form (% *α*–, % *β*– and % *δ*–mannitol) was performed by Rietveld refinement using Topas v4 (Bruker) software package. Cif structural models of mannitol polymorphs were obtained from the Cambridge Structural Database, refined within Topas on pure mannitol samples, and then converted to '.str' files. The area under the 'crystalline peaks' was measured for each PXRD diffractogram and used as a reference for the determination of relative degree of crystallinity. Assuming that the areas are proportional to the scattering intensities, the percent relative degree of crystallinity (RDC_{PXRD}) (Eq. 9) was estimated from the integrated relative intensities (*I*) of all 'crystalline peaks' and the amorphous region under the diffraction curve.

$$\mathbf{RDC_{PXRD}} = \mathbf{100} \times \frac{I_{\mathbf{crystalline}}}{I_{\mathbf{crystalline}} + I_{\mathbf{amorphous}}} \qquad \mathbf{(9)}.$$

The input to the intensity from the amorphous region ($I_{amorphous}$) was identified by accurately correcting the curvature of the background curve. The input to the intensity from the crystalline region ($I_{crystalline}$) was attained after deducting the background curve from the PXRD pattern. The reproducibility of the PXRD patterns was checked by performing four measurements of four different samples of each mannitol product.

2.11. Karl Fischer titration

The (residual) moisture content of LMs was determined by the Karl-Fisher method (Metter Toledo, C20 Coulometric KF Titrator, Switzerland). The Fischer reagent solution was Hydranal® Coulomat AF (Sigma-Aldrich, USA). Following the calibration of the instrument, samples were rapidly added into the titrator vessel at the laboratory temperature (22 ºC). The titration of each sample was repeated three times.

2.12. Preparation of tablets

Compression of mannitol powders was carried out using a single punch Specac press KBR 25.011 (Gemini BV, The Netherlands), fitted with 6 mm diameter flat–faced punches to produce

round tablets with a target weight of (100 ± 0.5) mg. Before compression, the compaction surfaces were lubricated with 1% (*w*/*v*) magnesium stearate (Acrõs Organics, New Jersey, USA) in acetone (Fisher Scientific, UK) to reduce the friction between the die and the tablet, and to prevent the produced tablets from sticking to the die walls and punch faces. Tablets were compressed at increasing compression pressures of 173, 346, 520, 693, 861 and 1040 MPa under load for 20 s dwell time. Tablet diameter and thickness were measured using a digital micrometer (Fisher Scientific, UK) immediately after ejection and 24 h after ejection to allow for elastic recovery and possible hardening of tablets. Tablets were stored in screw-capped glass vials (22 ºC, 50% RH). The results were the mean and standard deviation of five determinations.

2.13. Crushing strength and capping tendency

The crushing strength was determined from the force required to fracture the tablet by diametral compression on a motorised Vankel Tablet Hardness Tester (Model Bench Saver VK 200, USA). The tensile strength (TS) (Eq. 10) of each compact was calculated using the following equation (Fell and Newton, 1970).

$$\mathbf{TS} = \frac{\mathbf{2F}}{\boldsymbol{\pi} \mathbf{D_t}} \qquad \mathbf{(10)},$$

in which *D* and *t* are the diameter and thickness (mm) of the compact respectively, and *F* is the force exerted to fracture the compact. Tablets were assessed visually for capping by observation of the produced tablets for horizontal striations. Tests were carried out 24 h after ejection. Five tablets were selected for crushing strength measurements.

2.14. Preparation of mannitol–indomethacin formulations

LM powders were formulated with indomethacin, a model poorly water-soluble drug, to evaluate the in vitro dissolution performance of tablets containing LM in comparison to CM. Each tablet contained a mixture of 75 mg mannitol and 25 mg indomethacin (excipient to drug ratio of 3:1, *w*:*w*). The blending was performed in a cylindrical aluminium container (6.5 cm × 8 cm) using a Turbula® mixer (Maschinenfabrik, Basel, Switzerland) at a constant speed of 90 rpm for 30 min in laboratory conditions (22 ºC, RH = 50%) for the preparation of all formulations under a similar protocol. Once prepared, all formulations were stored in tightly sealed glass vials for 7 days (22 ºC, RH = 50%) before further operations to allow any possible charge relaxation to occur.

2.15. In vitro dissolution

A USP dissolution apparatus no. 1 (Erweka DT700, Germany) was used to monitor the in vitro dissolution profiles of indomethacin from tablets containing different mannitols compressed at a fixed pressure (173 MPa). The amounts of dissolved drug were analysed using a spectrophotometer (UV−160, Shimadzu, Japan) at 318 nm. The dissolution medium (900 mL of phosphate buffer of pH 7.2) was equilibrated to (37 ± 0.5) ºC at 50 rpm using the rotating paddle method. From the dissolution flasks, samples were withdrawn at predetermined time intervals (2, 4, 6, 8, 10, 15, 20, 25, 30, 35, 40, 50, 55, 60, 70, 80, 90, 100, 110 and 120 min). Three tablets were tested for each formulation.

2.16. Dissolution parameters

The dissolution efficiency (%DE, Eq. 11) was calculated from the area under the dissolution curve up to the time, *t*, expressed as the percentage of the area of the rectangle (Khan, 1975).

$$\mathbf{DE_t = \frac{\int_0^t y \times d_t}{y_{100} \times t} \times 100} \qquad \mathbf{(11)},$$

where *y* is the percent amount of the drug dissolved at time *t*. The mean dissolution time (MDT, Eq. 12) was calculated as the mean time for the drug to dissolve under in vitro dissolution conditions.

$$\mathbf{MDT = \frac{\sum_{j=1}^{n} t_j \Delta M_j}{\sum_{j=1}^{n} \Delta M_j}} \qquad \mathbf{(12)},$$

where j is the sample number, n is the number of dissolution sample times, t_j is the midpoint of the jth time period (calculated from [t+(t-1)/2]) and ΔM_j is the additional amount of the drug dissolved between t_j and t-1. The mean dissolution rate (MDR, Eq. 13) was calculated as the percent release of the drug every min using the following equation.

$$\mathbf{MDR = \frac{\sum_{j=1}^{n} \Delta M_j / \Delta_t}{n}} \qquad \mathbf{(13)},$$

where n is the number of dissolution times, Δt is the time at the midpoint between t and t−1 (calculated from [t + t−1)/2]) and ΔMj is the additional amount of the drug dissolved between tj and t−1. Additionally, as independent metrics, the mean percentage of the drug dissolved in the

first 4 min (Q_{4min}), 10 min (Q_{10min}), 30 min (Q_{30min}) and 50 min (Q_{50min}) were used to characterize the dissolution rate from various tablets.

2.17. Statistical analysis

One way analysis of variance (ANOVA) test was applied to compare the mean results for all data in this study considering P values less than 0.05 an as indicative of a significant difference. Data groups that showed a significant difference (ANOVA, P <0.05) were further subjected to the Tukey's post hoc test to identify which specific groups differed. The data are generally expressed as the mean ± standard deviation (SD).

3. Results and discussion

3.1. Density, porosity and cohesivity

Following freeze-drying, the true density of mannitol particles decreased (P <0.05) from (1.50 ± 0.02) g/cm^3 (CM) to the range between (1.19 ± 0.04) g/cm^3 and (1.45 ± 0.02) g/cm^3 (Table 1), indicating that LM particles do not have the same crystalline structure as CM. In comparison to CM, LMs demonstrated considerably lower bulk densities, lower tap densities, higher porosities, lower compactibilities and higher cohesivities (Table 1), indicating a lower number of average contact points between LM particles. This is because LMs exhibited loosely packed powder systems, leading to reduced interparticle contact areas and thus reduced interparticle forces as compared to CM. By comparing LMs only, regression analysis showed that by decreasing mannitol concentration, there was a decrease in the true density, bulk density (D_b, linear, r^2 = 0.9896), tap density (D_t, linear, r^2 = 0.99), along with an increase in porosity (linear, r^2 = 0.992) and cohesivity (1/b, r^2 = 0.8139) of LM products (Table 1). This is because the bulk density of the LM product depends on the freezing step. Freezing determine the dimension and the shape of the ice crystals that form the structure of the frozen LM product (Kochs et al., 1993; Nakagawa et al., 2006; Searles et al., 2001). Regardless of the concentration of mannitol solution, the LM powders were solids occupying approximately the volume of the former solution. Therefore, the volume of 1 g of mannitol increased from (1.8 ± 0.1) mL prior to lyophilisation

(i.e., CM) to a volume of (7.9 ± 0.3) mL, (11.8 ± 0.8) mL, (15.0 ± 0.4) mL and (34.0 ± 4.5) mL when lyophilised from 15%, 10%, 5% and 1% (*w*/*v*) mannitol respectively.

CM showed a good flow character (CI: 16.5% ± 0.8 %) whereas LMs demonstrated relatively poorer flow behaviours, characterized as fair (LM–15%), poor (LM–10% and LM–5%) and very poor (LM–1%) (Table 1). Plotting CI against mannitol concentration (C_{man}) indicated that the flowability of LM powders improved as mannitol concentration increased (Table 1). This is because the effect of gravity will be lower for mannitol particles lyophilised from lower concentrations owing to their lower density (Table 1).

3.2.Particle size and shape distributions

The size distributions of LM particles were strong functions of mannitol concentration (Table 2). The linear relationship (r^2 = 0.931) (Figure not shown) established between the median diameter ($d_{50\%}$) of LM and C_{man} indicated that the size of LM particles increased in response to decreasing mannitol concentration (Table 2), which is further confirmed by SEM images (Figure 1, SM–2). The variations in particle size distributions could be because the size of ice crystals is related to mannitol concentration. During the freezing, phase separation between water and mannitol, ice crystal growth, and solute cryo-concentration occur (Hottot et al., 2004). The growing ice crystals exclude mannitol molecules from its freezing front to the boundaries between neighbouring ice crystals. In the consequent drying process ice crystal sublimation and desorption of the bound water take place. The ice crystal growth depends on the adsorption/desorption balance of mannitol at the ice crystal surface (i.e., the adsorption and desorption of mannitol at the ice surface are in dynamic equilibrium). The effectiveness of a mannitol in inhibiting crystal growth depends on the extent of ice crystals' surface that is covered by mannitol. Therefore, high mannitol concentration leads to small crystals, whereas low mannitol concentration leads to large ones. The span values of 0.9 and 1.1 obtained for CM and LM–1% respectively (Table 2) indicated their narrow size distributions. The span of LM powders was inversely proportional to C_{man} (Table 2), indicating that the decrease in mannitol concentration linearly correlated with an increase in the size-homogeneity of LM particles, as further substantiated by SEM observations (Figure 1). This might be explained as a higher concentration of mannitol could induce more heterogeneous nucleation and less balanced speed of growth during particle forming, leading to higher polydispersity in particle size distribution. Good size-homogeneity (i.e. small span) of a

pharmaceutical formulation is usually desirable because it will recount directly to dose uniformity.

CM showed non-porous particles (Figure 1a) and hence particle true density is similar to particle density. LMs revealed fractured particles with wrinkled (corrugated) surfaces, producing open (rather than packed) particle structures (Figures 1b to e, SM–2). Such morphology increases the geometric interlocking among LM particles, further explaining their poorer flow properties in comparison to CM (Table 1). Microstructural observations with SEM supported the alternations in structural properties as a function of mannitol concentration. Mannitol particles lyophilised from concentrations ≤5% (*w*/*v*) showed macroporous surface texture characteristics composed of a microstructured network of particles with visible large pores and cavities (Figures 1e and d, SM–2). This is because lyophilisation process allows the ice to sublime, leaving voids within the structure without major shrinkage. Therefore, large pores were less evident within mannitol particles lyophilised from concentrations above 5% (*w*/*v*), although a hollow structure was observed (Figures 1b and c, SM–2). These remarkable morphological differences between the two groups of LM products (i.e. LM–1% and LM–5% *vs.* LM–10% and LM–15%) could be due a variation in the mechanism of crystal nucleation and propagation. The amount of pores created during freeze-drying is related to the water (i.e. ice) uptake process. A relatively higher degree of water (ice) uptake is expected during lyophilisation of solutions with lower concentrations and therefore the porosity of the lyophilised product becomes higher. Such porous structure observed for LM particles could explain their low true density (making them permeable for helium) and low bulk density in comparison to non-porous CM particles (Table 1).

3.3.Electrostatic charging

CM and mannitols lyophilised from concentrations above 5% (*w*/*v*) showed considerably higher levels of netcharge (from 2.2 to 4.8 nC/g) in comparison to mannitols lyophilised from concentrations ≤5% (*w*/*v*) (≤0.2 nC/g) (Figure 2a). The level netcharge of LM decreased with decreasing mannitol concentration (Figure 2a). A clear trend of decreased netcharge with increasing the median diameter of LM was established (Figure 2b). This could be attributed to the increase in the overall surface area available for charge-transfer in the case of smaller LM particles due to higher particle-wall contacts, greater particle number density, and higher surface area (Kaialy, 2016). High levels of electrostatic charging of pharmaceuticals intended for direct

compression is considered as a nuisance because it leads to their adherence to the punches, dies and feeding hopper, affecting tablet weight and hence drug content uniformity.

In contrast to CM, which showed a positive unipolar charging, all LMs showed remarkable bipolar charging behaviours (Figure 2a). For example, although the netcharge results showed that LM–1% carried almost no charge (0.1 nC/g), this sample recorded levels of 3.1 nC/g and −2.7 nC/g for P–CMR and N–CMR respectively (Figure 2a). This signifies that the measurement of the netcharge-to-mass ratio of a powder (using e.g. the Faraday pail method), where the process cause bipolar charging is not an accurate indicator for correlating the true charge-to-mass ratio.

3.4.Breakability

The median diameter ($d_{50\%}$) of LM particles decreased considerably with increasing the sonication time applied during measurements (Figure 3). This suggested that LM particles were fragile and suggestible to breakage with extended ultrasound application. This however does not offer information on the mechanism by which this reduction in particle size occurs. Therefore, the particle size of LM particles was determined at several time intervals at the end of the sonication process (200 s). The size of the sonicated LM particles did not return to its original size (data not shown). This suggested that the decrease in particle size upon sonication is attributable to the fracturing of brittle individual LM particles. For each mannitol product, the particle size profile reached a plateau at a particular sonication time, after which relatively 'stable' (P >0.05) size descriptors were obtained (Figure 3). From Figure 3, it can be seen that LM particles produced steeper decreases in sizes as a function of the increase in sonication time as compared to CM. Due to their increased angularity (Figure 1, SM–2), LM particles could have increased damage caused because of stress (Sadrekarimi and Olson, 2010). Therefore, in comparison to CM, LMs demonstrated considerably higher relative degrees of breakage (RDB), with the RDB increasing with decreasing mannitol concentration (Figure 3). This could be ascribed to the increased brittleness for mannitols lyophilised from lower concentrations in comparison to mannitols lyophilised from higher concentrations due to their relatively more porous structure and larger size (Table 1; Figure 1).

3.5.Solid-state

LM samples produced parallel DSC traces with endothermic transitions ranging from (168.2 ± 0.3) ºC to (169.7 ± 1.2) ºC (mean ± SD, P >0.05) (Figure 4), corresponding to the melting point of the two orthorhombic polymorphs, i.e., α− or β−mannitol (Burger et al., 2000). The presence of the diagnostic FT−IR bands of both α− (1194 cm^{-1}, 1370 cm^{-1} and 1388 cm^{-1}) and β– (929 cm^{-1} and 959 cm^{-1}) mannitol (Burger et al., 2000) in the FT–IR spectra of all LMs confirmed that they all contained both α and β forms (Figure 5). Mannitols lyophilised from concentrations ≤5% (*w*/*v*) exhibited an additional minor DSC endotherm with melting peaks ranging from (150.1 ± 0.1) ºC to (152.5 ± 4.2) ºC (mean ± SD, P >0.05), which is symptomatic to the presence of the monoclinic δ–mannitol (Burger et al., 2000; Kaialy et al., 2015). Such transition however was not observed in the DSC trace LM–10% and it was trivial for LM–15% (Figure 4). This was in accordance with FT−IR analysis, in which the δ–mannitol characteristic band (967 cm^{-1}) was only visible in LM–1% and LM–5% (Figure 5). LMs demonstrated lower calorimetric melting enthalpies (from 259.1 J/g ± 3.8 J/g to 282.4 J/g ± 0.8 J/g) than CM (315.3 J/g ± 6.1 J/g) (Figure 4). Comparing LMs only showed that the melting enthalpy of mannitol decreased (linearly, r^2 = 0.9521, Figure not shown) with decreasing the concentration of mannitol (Figure 4). In addition, in comparison to CM, LM–1% exhibited broader FT−IR bands in the fingerprint region from 1200 cm^{-1} to 1500 cm^{-1} (Figure 5). Accordingly, both DSC and FT−IR analyses suggested that freeze-drying produced some defects in the structural lattice of mannitol, particularly in the case of low mannitol concentrations. The residual moisture measured for the mannitol lyophilisates was insignificant (0.2% ± 0.1%, *w*/*w*) which is ideal for storage stability (Barresi et al., 2009; Tang and Pikal, 2004). This agrees with DSC analysis that showed no endothermic transitions below 100 ºC for all mannitols (Figure 4), confirming the absence of detectable surface (free) water (which would have produced an endotherm at ~ 100 °C) or metastable monoclinic mannitol hemihydrate (which would have produced an endotherm at ~ 80 °C (Liao et al., 2007)).

PXRD analyses verified that all LMs contained mixtures of α–, β– and δ–mannitol in different quantities (Figure 6a). Mannitols lyophilised from concentrations above 5% (*w*/*v*) were shown by PXRD to have less amounts of δ–mannitol than mannitols lyophilised from concentrations ≤5% (*w*/*v*) (Figure 6a). It was clear that such low amounts of δ–mannitol were not detected by either DSC (because the melting point of δ–mannitol is close to the melting point of

α– and *β*–mannitol (Takada et al., 2009)) or FT−IR (probably because FT−IR analysis is limited to detecting a thin layer of only 1 μm). Plotting % *δ*–mannitol content assessed by PXRD against *δ*–mannitol transition enthalpy assessed by DSC resulted in a direct linear relationship (r^2 = 0.9903) (Figure 6b) indicating that the two techniques were in concurrence. Additionally, the order of % crystalline fraction analysis assessed using PXRD corresponded to % crystalline fraction analysis assessed using DSC (Figure 6c), both confirming that LMs have lower relative degrees of crystallinities (RDCs) in comparison to CM. Yet, the slight variations in the absolute % crystallinity data between DSC and PXRD could be attributed to the pronounced differences between DSC and PXRD techniques in terms of sample geometry, sample size, temperature program, etc. The RDC of LM decreased as the concentration of mannitol decreased (Figure 6c). This could be because an increase in the mannitol concentration enhances the crystallization behavior of LM (Kim et al., 1998). The reduced RDC of mannitols lyophilised from lower concentrations, in comparison to mannitols lyophilised from higher concentrations, could explain their lower true densities due to increased mobility (Kikuchi et al., 2011).

3.6.Mechanical properties

The compaction pressure played a significant role on the mechanical strength of LM tablets (Figure 7a). In general, the tensile strength (TS) of all tablets showed a decreasing trend with increasing the compression pressure (Figure 7a). It is also clear from Figure 7a that the TS of LM tablets are increased with decreasing mannitol concentration. This indicates stronger interparticle bonding between LM particles lyophilised from lower concentrations in comparison to LM particles lyophilised from higher concentrations, attributable to their different structural characteristics. It has been shown that *δ*–mannitol achieve superior tabletting performance as compared to *β*–mannitol (Yoshinari, 2003). Therefore, the presence of *δ*–mannitol in LMs (Figure 6) could be one of the reasons for the improvement in the mechanical properties of LM tablets in comparison to CM tablets. However, although all LMs contained a portion of *δ*–mannitol, mannitols lyophilised from 15% (*w*/*v*) concentration did not show improved compactibility in comparison to CM (*β*–mannitol) (Figure 7a). This indicates that there are other factors in play. The more porous structure of mannitols lyophilised from lower concentrations (Table 1; Figure 1) contribute to their improved tabletability in comparison to mannitols lyophilised from higher concentrations. This is because the increase in powder bed porosity allows particle–particle interactions of greater extent during the subsequent stage of compression, resulting in higher

tabletability (Westermarck et al., 1998). Additionally, the lower relative degrees of crystallinity of mannitols lyophilised from lower concentrations in comparison to mannitols lyophilised from higher concentrations (Figure 6c) could be another reason for the higher tensile strengths for tablets made from mannitols lyophilised from lower concentrations. Moreover, the higher breakability of mannitols lyophilised from lower concentrations (in comparison to mannitols lyophilised from higher concentrations) (Figure 3) result in larger relative volume changes during the early stage of compression due to their fragmentation, producing tablets with higher tabletability. Plotting the TS of LM tablets against the RDC and RDB confirmed that mannitols with lower relative degrees of crystallinity (Figure 7b) and higher relative degrees of breakage (Figure 7c) generated tablets with better mechanical properties.

3.7.Dissolution studies

The dissolution rate of indomethacin tablets was enhanced when formulated with LM (in the form of a physical mix) (Figure 8). Such enhancement could be attributed to the betterment of indomethacin wettability due to the presence of relatively less crystalline (Figure 6) and highly porous (Table 1, Figure 1, SM–2) LM, which provides high surface area available for drug dissolution and a potentially increased abundance of polar groups. Regression analysis (Figures not shown) revealed that the DE (r^2 = 0.9793) and MDR (r^2 = 0.8994) have linearly increased, whereas MDT has linearly decreased (r^2 = 0.9395), with decreasing the concentration of mannitol (Table 3). This could be attributed to the increased porosity (Table 1, Figure 1, SM–2) and decreased crystallinity (Figure 6) for mannitols lyophilised from lower concentrations in comparison to mannitols lyophilised from higher concentrations. The low Van der Waals forces between drug and LM particles (due to the high porosity of LM) could increase the effective surface area for dissolution resulting in an enhanced drug dissolution rate.

Two groups of dissolution profiles could be observed for the LM–indomethacin formulations. Mannitols lyophilised from concentrations ≤5% (*w*/*v*) generated noticeably better dissolution rates of indomethacin than mannitols lyophilised from concentrations above 5% (*w*/*v*) (Figure 8). Mannitols lyophilised from concentrations ≤ 5% (*w*/*v*) showed a lack of significant difference (P >0.05) between the amounts of indomethacin dissolved after 4 min (Q_{4min}), 10 min (Q_{10min}), 30 min (Q_{30min}) and 50 min (Q_{50min}) (Table 3). Similarly, mannitols lyophilised from concentrations above 5% (*w*/*v*) produced similar (P >0.05) amounts of indomethacin dissolved

after 4 min (Q_{4min}) and 10 min (Q_{10min}) (Table 3). Such results could be related to the presence of two populations of morphologies of LM. Macroporous structures were observed in the case of LM–1% and LM–5% (Figures 1 and d) but not in the case of LM–10% and LM–15% (Figures 1c and b, SM−3). LM–1% produced the fastest dissolution profile of indomethacin with a complete dissolution after 80 min, whereas CM produced the slowest pattern of dissolution of indomethacin with only 33% of indomethacin being dissolved at the same time (Figure 8). In comparison to CM, LM–1% produced a 3.5 fold increase in the dissolution efficiency (DE: 25.1% ± 3.3% versus 87.5% ± 0.4%) and a 4.7 fold increase in the mean dissolution rate (MDR: 0.27 min^{-1} ± 0.06 min^{-1} versus 1.25 min^{-1} ± 0.07 min^{-1}) of indomethacin (Table 3).

Further studies could be performed to establish the influence of mannitol concentration on the physicochemical, mechanical and pharmaceutical properties of LM at varying lyophilisation protocols (e.g., different controlled cooling rates) and formulated with a wider range of drugs intend for both oral and pulmonary drug delivery. It would also be of interest to evaluate the effects of annealing conditions on the physicochemical (e.g. pore size) and mechanical properties of lyophilised mannitol products that showed a reduced relative degree of crystallinity (i.e., LM-1%).

4. Summary and conclusions

The micro- and macro-structural changes of mannitol products lyophilised from solutions having different concentrations can be predicted. By decreasing mannitol concentration, the density, flowability and crystallinity of lyophilised mannitol were decreased, whereas the porosity and breakability (fragility) of lyophilised mannitol were increased. Clear trends of improved mechanical properties and enhanced dissolution rates were established with decreasing the concentration of mannitol solution subjected to freeze-drying. The formulators could therefore optimize the mechanical and dissolution properties of LM tablets via the careful selection of mannitol concentration prior to freeze-drying.

This work recommends the use of mannitol lyophilised from 1% (*w*/*v*) mannitol for the preparation of directly compressible preparation with excellent mechanical and rapid dissolution properties. Mannitol particles lyophilised from the lowest concentration (1%, *w*/*v*) were ultra-

fluffy (bulk density of only 0.03 g/cm^3), porous, flake-shaped, and produced the best tablets with ×9.1 fold increase in tablet tensile strength (5.04 MPa versus 0.56 MPa) and ×3.5 fold increase of dissolution efficiency (87.5% versus 25.1%) of indomethacin in comparison to commercial mannitol. Further optimisation of the utilization of lyophilisation in the design of mannitol particles with desired pharmaceutical properties should be considered.

Acknowledgements

David Townrow (University of Wolverhampton) and Tariq Hussain (University of Greenwich) for carrying out the PXRD and electrostatic charge experiments respectively.

References

Ahlneck, C., Zografi, G., 1990. The molecular basis of moisture effects on the physical and chemical stability of drugs in the solid state. Int. J. Pharm. 62, 87–95. doi:10.1016/0378-5173(90)90221-O

Barresi, A.A., Ghio, S., Fissore, D., Pisano, R., 2009. Freeze Drying of Pharmaceutical Excipients Close to Collapse Temperature: Influence of the Process Conditions on Process Time and Product Quality. Dry. Technol. 27, 805–816. doi:10.1080/07373930902901646

Bauer, H., Herkert, T., Bartels, M., Kovar, K.A., Schwarz, E., Schmidt, P.C., 2000. Investigations on polymorphism of mannitol/ sorbitol mixtures after spray-drying using Differential scanning calorimetry, X-ray diffraction and Near-Infrared spectroscopy. Pharm. Ind. 62, 231–235.

Berman, H.M., Jeffrey, G.A., Rosenstein, R.D., 1968. The crystal structures of the α' and β forms of D-mannitol. Acta Crystallogr. Sect. B Struct. Crystallogr. Cryst. Chem. 24, 442–449.

Bharate, S.S., Bharate, S.B., Bajaj, A.N., 2010. Incompatibilities of Pharmaceutical Excipients with Active Pharmaceutical Ingredients: A Comprehensive Review. J. Excipients Food Chem.

Blagden, N., de Matas, M., Gavan, P.T., York, P., 2007. Crystal engineering of active pharmaceutical ingredients to improve solubility and dissolution rates. Adv. Drug Deliv. Rev. 59, 617–30. doi:10.1016/j.addr.2007.05.011

Botez, C.E., Stephens, P.W., Nunes, C., Suryanarayanan, R., 2003. Crystal structure of anhydrous δ-D-mannitol. Powder Diffr. 18, 214–218. doi:10.1154/1.1582460

Brodka-Pfeiffer, K., Langguth, P., Graβ, P., Häusler, H., 2003. Influence of mechanical activation on the physical stability of salbutamol sulphate. Eur. J. Pharm. Biopharm. 56, 393–400.

Burger, A., Henck, J.O., Hetz, S., Rollinger, J.M., Weissnicht, A.A., Stöttner, H., 2000. Energy/temperature diagram and compression behavior of the polymorphs of D-mannitol. J.

Pharm. Sci. 89, 457–68. doi:10.1002/(SICI)1520-6017(200004)89:4<457::AID-JPS3>3.0.CO;2-G

Cannon, A., Trappler, E., 1999. The influence of lyophilization on the polymorphic behavior of mannitol. PDA J. Pharm. Sci. 54, 13–22.

Cao, W., Mao, C., Chen, W., Lin, H., Krishnan, S., Cauchon, N., 2006. Differentiation and quantitative determination of surface and hydrate water in lyophilized mannitol using NIR spectroscopy. J. Pharm. Sci. 95, 2077–86. doi:10.1002/jps.20706

Cavatur, R.K., Suryanarayanan, R., 1998. Characterization of Phase Transitions During Freeze-Drying by In Situ X-ray Powder Diffractometry. Pharm. Dev. Technol. 3, 579–586.

Cavatur, R.K., Vemuri, N.M., Pyne, A., Chrzan, Z., Toledo-Velasquez, D., Suryanarayanan, R., 2002. Crystallization Behavior of Mannitol in Frozen Aqueous Solutions. Pharm. Res. 19, 894–900. doi:10.1023/A:1016177404647

De Beer, T.R.M., Allesø, M., Goethals, F., Coppens, A., Heyden, Y. Vander, De Diego, H.L., Rantanen, J., Verpoort, F., Vervaet, C., Remon, J.P., Baeyens, W.R.G., 2007. Implementation of a process analytical technology system in a freeze-drying process using Raman spectroscopy for in-line process monitoring. Anal. Chem. 79, 7992–8003. doi:10.1021/ac070549h

De Beer, T.R.M., Vercruysse, P., Burggraeve, A., Quinten, T., Ouyang, J., Zhang, X., Vervaet, C., Remon, J.P., Baeyens, W.R.G., 2009. In-line and real-time process monitoring of a freeze drying process using Raman and NIR spectroscopy as complementary process analytical technology (PAT) tools. J. Pharm. Sci. 98, 3430–46. doi:10.1002/jps.21633

Eadala, P., Waud, J.P., Matthews, S.B., Green, J.T., Campbell, A.K., 2009. Quantifying the 'hidden' lactose in drugs used for the treatment of gastrointestinal conditions. Aliment. Pharmacol. Ther. 29, 677–87. doi:10.1111/j.1365-2036.2008.03889.x

EMA, 2002. Public report: risk an regulatory assessment of lactose and other products prepared using calf rennet. London.

Fell, J.T., Newton, J.M., 1970. Determination of tablet strength by the diametral-compression test. J. Pharm. Sci. 59, 688–691. doi:10.1002/jps.2600590523

Franks, F., Auffret, T., 2008. Freeze-drying of Pharmaceuticals and Biopharmaceuticals. Royal Society of Chemistry.

Franks, F., Aufrett, T., 2007. Freeze-drying/lyophilisation of pharmaceutical and biological products, principles and practice. London: RSC Publishing.

Gan, K.H., Bruttini, R., Crosser, O.K., Liapis, A.I., 2004. Heating Policies during the Primary and Secondary Drying Stages of the Lyophilization Process in Vials: Effects of the Arrangement of Vials in Clusters of Square and Hexagonal Arrays on Trays. Dry. Technol. 22, 1539–1575. doi:10.1081/DRT-200025596

Geil, P., 1996. Complex and simple carbohydrates in diabetes therapy, in: Powers, M. (Ed.), Handbook of Diabetes Medical Nutrition Therapy. Gaithersburg: Aspen Publishers.

Haikala, R., Eerola, R., 1997. Polymorphic changes of mannitol during freeze-drying: effect of surface-active agents. PDA J. Pharm. Sci. Technol. 51, 96–101.

Hottot, A., Nakagawa, K., Andrieu, J., 2008. Effect of ultrasound-controlled nucleation on structural and morphological properties of freeze-dried mannitol solutions. Chem. Eng. Res. Des. 86, 193–200.

Hottot, A., Vessot, S., Andrieu, J., 2004. A Direct Characterization Method of the Ice Morphology. Relationship Between Mean Crystals Size and Primary Drying Times of Freeze-Drying Processes. Dry. Technol. 22, 2009–2021. doi:10.1081/DRT-200032717

Hussain, T., Deng, T., Bradley, M., Chelu, D., Gorman, T., Kaialy, W., 2016. Evaluation studies of a sensing technique for electrostatic charge polarity of pharmaceutical particulates. IET Sci. Meas. Technol. In press. doi:10.1049/iet-smt.2015.0194

Hussain, T., Kaialy, W., Deng, T., Bradley, M.S.A., Nokhodchi, A., Armour-Chélu, D., 2013. A novel sensing technique for measurement of magnitude and polarity of electrostatic charge distribution across individual particles. Int. J. Pharm. 441, 781–789.

Izutsu, K., Yoshioka, S., Terao, T., 1994. Effect of Mannitol Crystallinity on the Stabilization of Enzymes during Freeze-Drying. Chem. Pharm. Bull. 42, 5–8. doi:10.1248/cpb.42.5

Kaialy, W., 2016. A review of factors affecting electrostatic charging of pharmaceuticals and adhesive mixtures for inhalation. Int. J. Pharm. 503, 262–276. doi:10.1016/j.ijpharm.2016.01.076

Kaialy, W., Al Shafiee, M., 2015. Recent advances in the engineering of nanosized active pharmaceutical ingredients: promises and challenges. Adv. Colloid Interface Sci. 228, 71–91. doi:10.1016/j.cis.2015.11.010

Kaialy, W., Larhrib, H., Chikwanha, B., Shojaee, S., Nokhodchi, A., 2014. An approach to engineer paracetamol crystals by antisolvent crystallization technique in presence of various additives for direct compression. Int. J. Pharm. 464, 53–64.

Kaialy, W., Larhrib, H., Ticehurst, M., Nokhodchi, A., 2012. Influence of batch cooling crystallization on mannitol physical properties and drug dispersion from dry powder inhalers. Cryst. Growth Des. 12, 3006–3017.

Kaialy, W., Martin, G.P., Ticehurst, M.D., Momin, M.N., Nokhodchi, A., 2010. The enhanced aerosol performance of salbutamol from dry powders containing engineered mannitol as excipient. Int. J. Pharm. 392, 178–188.

Kaialy, W., Nokhodchi, A., Larhrib, H., Martin, G.P., Nokhodchi, A., 2015. Dry powder inhalers: Physicochemical and aerosolization properties of several size-fractions of a promising alterative carrier, freeze-dried mannitol. Eur. J. Pharm. Sci. 68, 56–67.

Kawakita, K., Lüdde, K.-H., 1971. Some considerations on powder compression equations. Powder Technol. 4, 61–68. doi:10.1016/0032-5910(71)80001-3

Khan, K.A., 1975. The concept of dissolution efficiency. J. Pharm. Pharmacol. 27, 48–49. doi:10.1111/j.2042-7158.1975.tb09378.x

Kikuchi, T., Wang, B.S., Pikal, M.J., 2011. High-precision absolute (true) density measurements on hygroscopic powders by gas pycnometry: application to determining effects of formulation and process on free volume of lyophilized products. J. Pharm. Sci. 100, 2945–51. doi:10.1002/jps.22521

Kim, A., Akers, M., Nail, S., 1998. The physical state of mannitol after freeze- drying: Effects of mannitol concentration, freezing rate, and a noncrystallizing cosolute. J. Pharm. Sci.

Kim, H.S., Jeffrey, G.A., Rosenstein, R.D., 1968. The crystal structure of the K form of D-mannitol. Acta Crystallogr. Sect. B Struct. Crystallogr. Cryst. Chem. 24, 1449–1455. doi:10.1107/S0567740868004462

Kochs, M., Körber, C., Heschel, I., Nunner, B., 1993. The influence of the freezing process on vapour transport during sublimation in vacuum-freeze-drying of macroscopic samples. Int. J. Heat Mass Transf. 36, 1727–1738. doi:10.1016/S0017-9310(05)80159-0

Lawson, M., 2000. Sugar alcohols, in: Kirk-Othmer Encyclopedia of Chemical Technology. John Wiley & Sons Inc., New York, pp. 93–119.

Liao, X., Krishnamurthy, R., Suryanarayanan, R., 2007. Influence of processing conditions on the physical state of mannitol--implications in freeze-drying. Pharm. Res. 24, 370–6. doi:10.1007/s11095-006-9158-3

Nakagawa, K., Hottot, A., Vessot, S., Andrieu, J., 2006. Influence of controlled nucleation by ultrasounds on ice morphology of frozen formulations for pharmaceutical proteins freeze-drying. Chem. Eng. Process. Process Intensif. 45, 783–791. doi:10.1016/j.cep.2006.03.007

Nunes, C., Suryanarayanan, R., Botez, C.E., Stephens, P.W., 2004. Characterization and crystal structure of D-mannitol hemihydrate. J. Pharm. Sci. 93, 2800–9. doi:10.1002/jps.20185

Oddone, I., Van Bockstal, P.-J., De Beer, T., Pisano, R., 2016. Impact of vacuum-induced surface freezing on inter- and intra-vial heterogeneity. Eur. J. Pharm. Biopharm. In press. doi:10.1016/j.ejpb.2016.04.002

Ohrem, H.L., Schornick, E., Kalivoda, A., Ognibene, R., 2014. Why is mannitol becoming more and more popular as a pharmaceutical excipient in solid dosage forms? Pharm. Dev. Technol. 19, 257–62. doi:10.3109/10837450.2013.775154

Parrott, E.L., 1990. Comminution. Encycl. Pharm. Technol. 3, 101–121.

Picksak, G., Stichtenoth, D.O., 2009. [Lactose-containing tablets for patients with lactose intolerance?]. Medizinische Monatsschrift für Pharm. 32, 27–8.

Pikal, M., 2002. Freeze drying, in: Swarbrick, J., Boylan, J. (Eds.), Encyclopedia of Pharmaceutical Technology. New York: Marcel Dekker, pp. 1807–1833.

Pikal-Cleland, K.A., Rodríguez-Hornedo, N., Amidon, G.L., Carpenter, J.F., 2000. Protein Denaturation during Freezing and Thawing in Phosphate Buffer Systems: Monomeric and Tetrameric β-Galactosidase. Arch. Biochem. Biophys. 384, 398–406. doi:10.1006/abbi.2000.2088

Pisano, R., Rasetto, V., Barresi, A.A., Kuntz, F., Aoude-Werner, D., Rey, L., 2013. Freeze-drying of enzymes in case of water-binding and non-water-binding substrates. Eur. J. Pharm. Biopharm. Off. J. Arbeitsgemeinschaft für Pharm. Verfahrenstechnik e.V 85, 974–83. doi:10.1016/j.ejpb.2013.02.008

Rasenack, N., Müller, D. (hon) B.W., 2004. Micron-Size Drug Particles: Common and Novel Micronization Techniques. Pharm. Dev. Technol.

Rene, F., Wolff, E., Rodolphe, F., 1993. Vacuum freeze-drying of a liquid in a vial: determination of heat and mass-transfer coefficients and optimisation of operating pressure. Chem. Eng. Process. Process Intensif. 32, 245–251. doi:10.1016/0255-2701(93)80006-3

Rogers, T.L., Nelsen, A.C., Sarkari, M., Young, T.J., Johnston, K.P., III, R.O.W., 2003. Enhanced Aqueous Dissolution of a Poorly Water Soluble Drug by Novel Particle Engineering Technology: Spray-Freezing into Liquid with Atmospheric Freeze-Drying. Pharm. Res. 20, 485–493. doi:10.1023/A:1022628826404

Romero-Torres, S., Wikstrom, H., Grant, E.R., Taylor, L.S., 2007. Monitoring of Mannitol Phase Behavior during Freeze-Drying Using Non-Invasive Raman Spectroscopy. PDA J. Pharm. Sci. Technol. 61, 131–145.

Sadrekarimi, A., Olson, S.M., 2010. Particle damage observed in ring shear tests on sands. Can. Geotech. J. 47, 497–515. doi:10.1139/T09-117

Searles, J.A., Carpenter, J.F., Randolph, T.W., 2001. The ice nucleation temperature determines the primary drying rate of lyophilization for samples frozen on a temperature-controlled shelf. J. Pharm. Sci. 90, 860–871. doi:10.1002/jps.1039

Snow, R., Kaye, B., Capes, C., Sresty, G., 1984. Size reduction and size enlargement, in: Perry, R.H., Green, D. (Eds.), Perry's Chemical Engineer's Handbook. McGraw Hill, New York, pp. 1–59.

Steckel, H., Markefka, P., teWierik, H., Kammelar, R., 2006. Effect of milling and sieving on functionality of dry powder inhalation products. Int. J. Pharm. 309, 51–9. doi:10.1016/j.ijpharm.2005.10.043

Takada, A., Nail, S.L., Yonese, M., 2009. Influence of ethanol on physical state of freeze-dried mannitol. Pharm. Res. 26, 1112–20. doi:10.1007/s11095-009-9829-y

Tang, X., Pikal, M., 2004. Design of freeze-drying processes for pharmaceuticals: practical advice. Pharm. Res.

Telang, C., Suryanarayanan, R., Yu, L., 2003. Crystallization of D-Mannitol in Binary Mixtures with NaCl: Phase Diagram and Polymorphism. Pharm. Res. 20, 1939–1945. doi:10.1023/B:PHAM.0000008040.14958.bc

Tong, H.H.Y., Chow, A.H.L., 2006. Control of Physical Forms of Drug Particles for Pulmonary Delivery by Spray Drying and Supercritical Fluid Processing. KONA Powder Part. J. 24, 27–40. doi:10.14356/kona.2006007

Vehring, R., 2008. Pharmaceutical particle engineering via spray drying. Pharm. Res. 25, 999–1022.

Velardi, S.A., Barresi, A.A., 2008. Development of simplified models for the freeze-drying process and investigation of the optimal operating conditions. Chem. Eng. Res. Des. 86, 9–22. doi:10.1016/j.cherd.2007.10.007

Vromans, H., 1987. Studies on consolidation and compaction properties of lactose. University of Groningen (Groningen, The Netherlands).

Walter-Levy, L., 1968. Cristallochimie-sur les variétés cristallines du D-mannitol. CR Acad Sc Paris Ser C 267, 1779–82.

Westermarck, S., Juppo, A.M., Kervinen, L., Yliruusi, J., 1998. Pore structure and surface area of mannitol powder, granules and tablets determined with mercury porosimetry and nitrogen adsorption. Eur. J. Pharm. Biopharm. 46, 61–68. doi:10.1016/S0939-6411(97)00169-0

Yoshinari, T., 2003. The improved compaction properties of mannitol after a moisture-induced polymorphic transition. Int. J. Pharm. 258, 121–131. doi:10.1016/S0378-5173(03)00157-1

Yu, L., Milton, N., Groleau, E.G., Mishra, D.S., Vansickle, R.E., 1999. Existence of a mannitol hydrate during freeze-drying and practical implications. J. Pharm. Sci. 88, 196–8.

Zeng, X.M., Martin, G.P., Marriott, C., Pritchard, J., 2000. The Influence of Crystallization Conditions on the Morphology of Lactose Intended for Use as a Carrier for Dry Powder Aerosols. J. Pharm. Pharmacol. 52, 633–643. doi:10.1211/0022357001774462

Zumbe, A., Lee, A., Storey, D., 2001. Polyols in confectionery: the route to sugar-free, reduced sugar and reduced calorie confectionery. Br. J. Nutr. 85, 31–45.

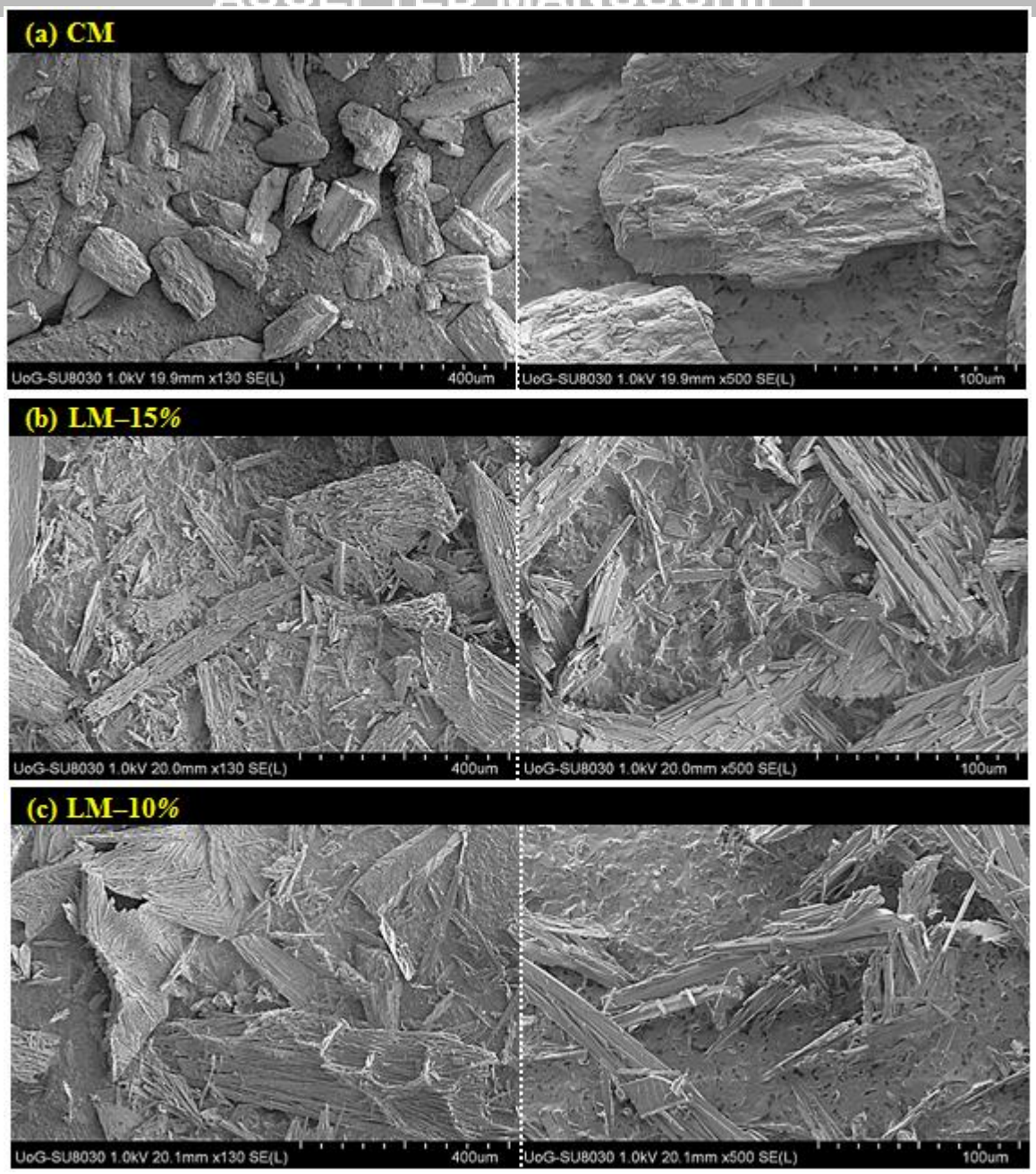

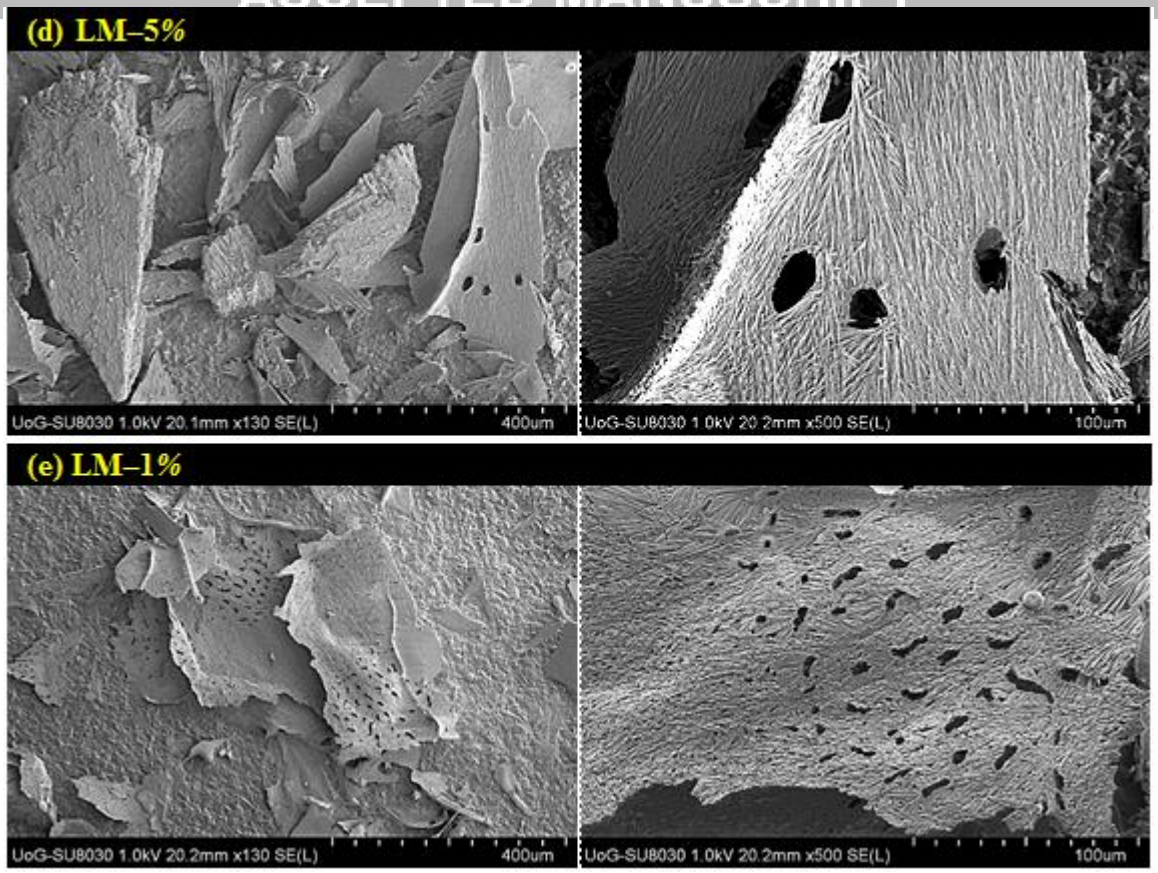

Figure 1. Representative scanning electron microscope (SEM) images commercial mannitol (CM) (**a**) and mannitol lyophilised from a series of mannitol solutions with different concentrations, i.e., 1% (LM–1%) (**b**), 5% (LM–5%) (**c**), 10% (LM–10%) (**d**), and 15% (LM–15%) *w*/*v* (**e**).

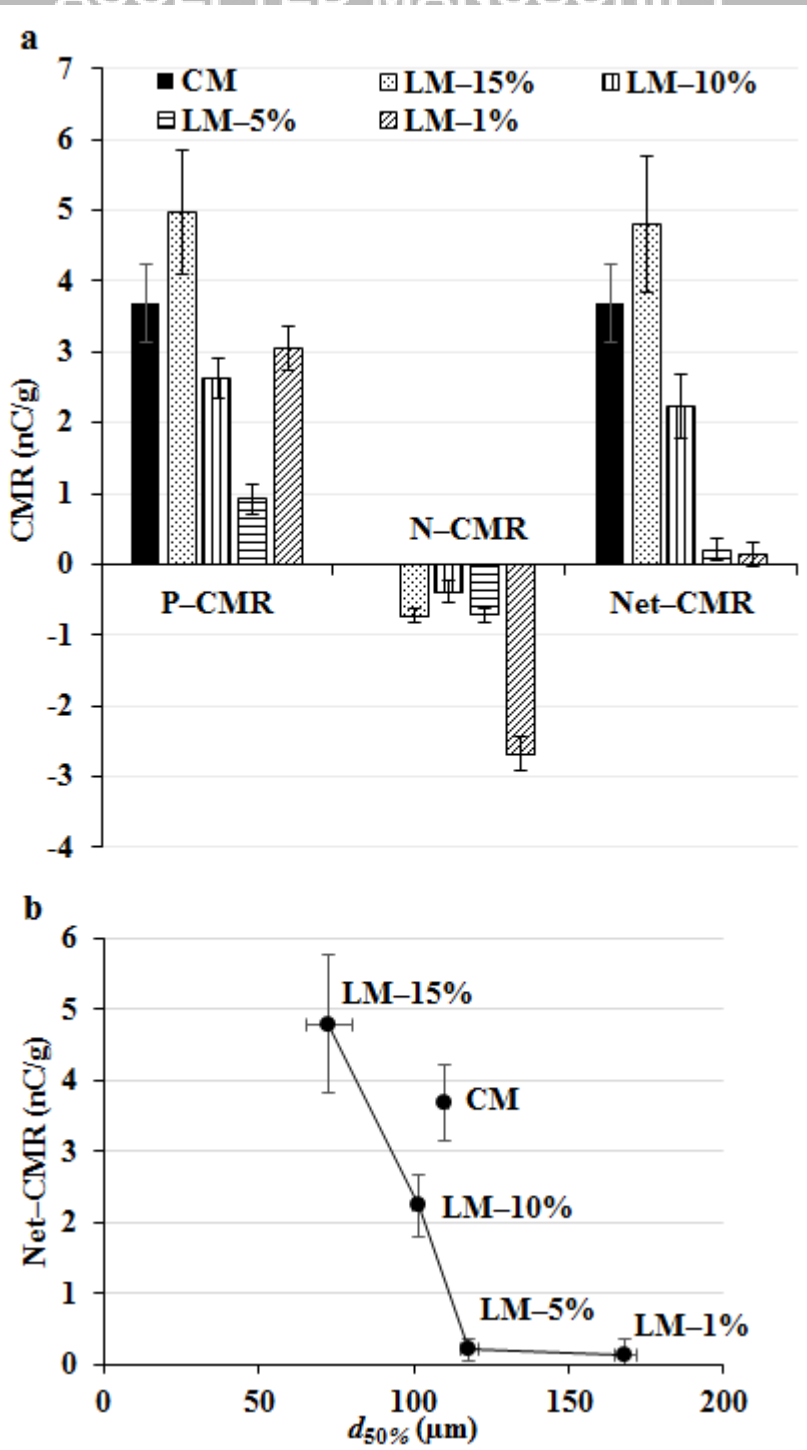

Figure 2. Positive charge-to-mass ratio (P–CMR), negative charge-to-mass ratio (N–CMR) and net charge-to-mass ratio (Net–CMR) (mean ± SD, n = 6) (**a**); and net–CMR in relation to median diameter ($d_{50\%}$) (**b**) of commercial mannitol (CM) and mannitol lyophilised from a series of mannitol solutions with different concentrations, i.e., 15% (LM–15%), 10% (LM–10%), 5% (LM–5%) and 1% *w*/*v* (LM–1%).

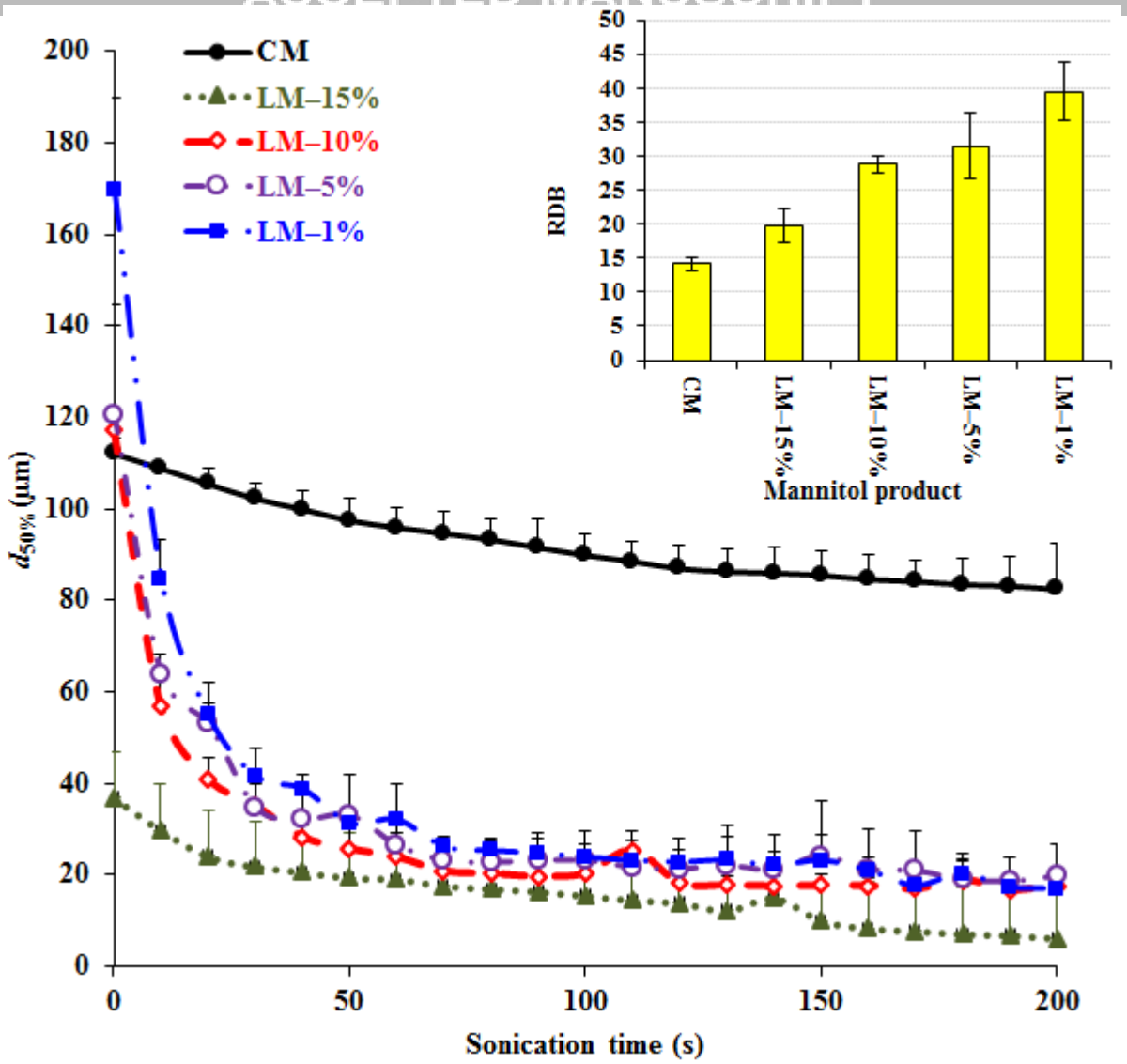

Figure 3. Median diameter ($d_{50\%}$) in relation to sonication time applied during wet-dispersion and relative degree of breakage (RDB) of (●) commercial mannitol (CM) and mannitol lyophilised from a series of mannitol solutions with different concentrations, i.e., 15% (▲, LM–15%), 10% (◊, LM–10%), 5% (○, LM–5%) and 1% *w*/*v* (■, LM–1%).

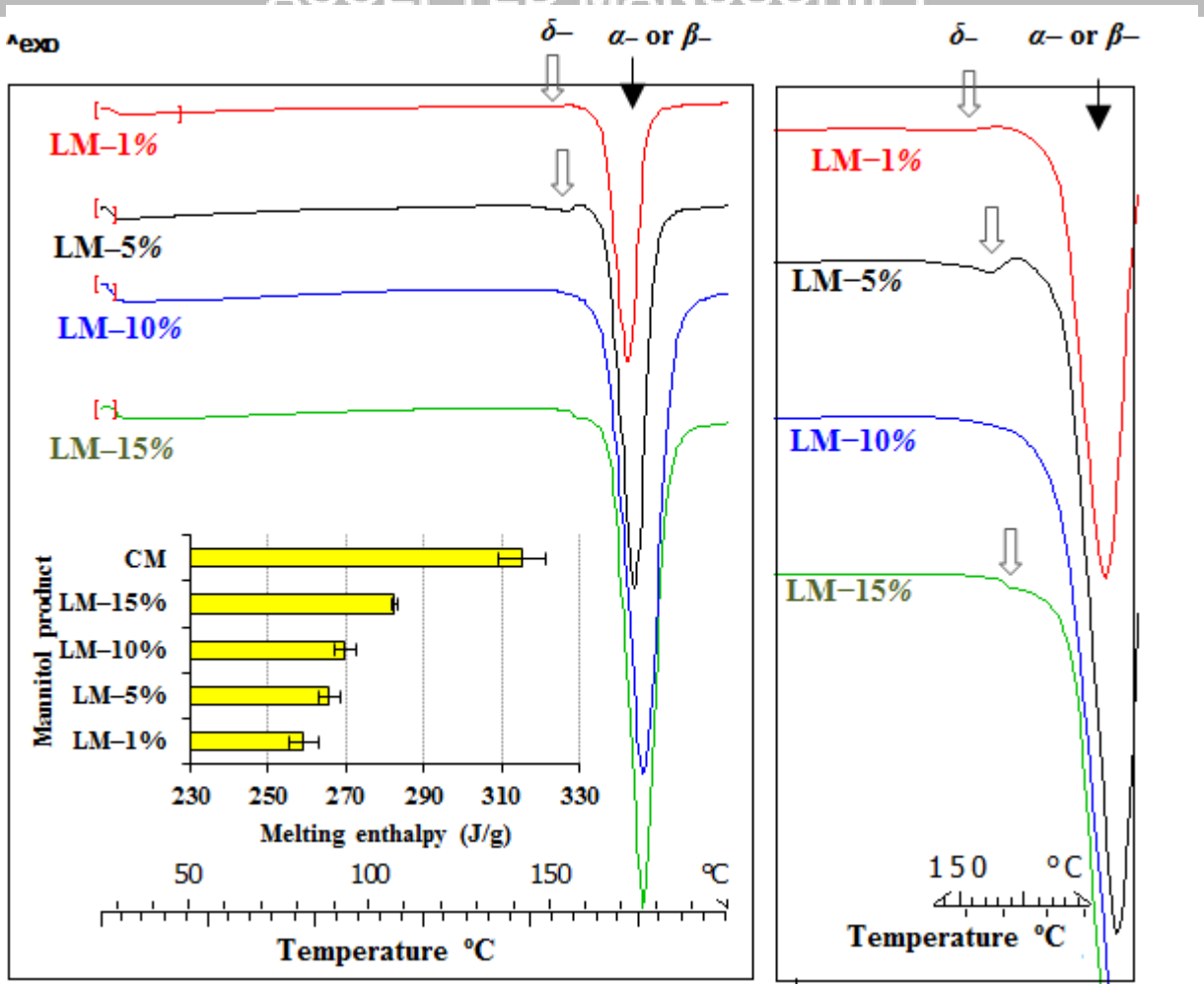

Figure 4. Differential scanning calorimetry (DSC) traces and melting enthalpies (mean ± SD, *n* = 4) of commercial mannitol (CM) and mannitol lyophilised from a series of mannitol solutions with different concentrations, i.e., 15% (LM–15%), 10% (LM–10%), 5% (LM–5%) and 1% *w*/*v* (LM–1%).

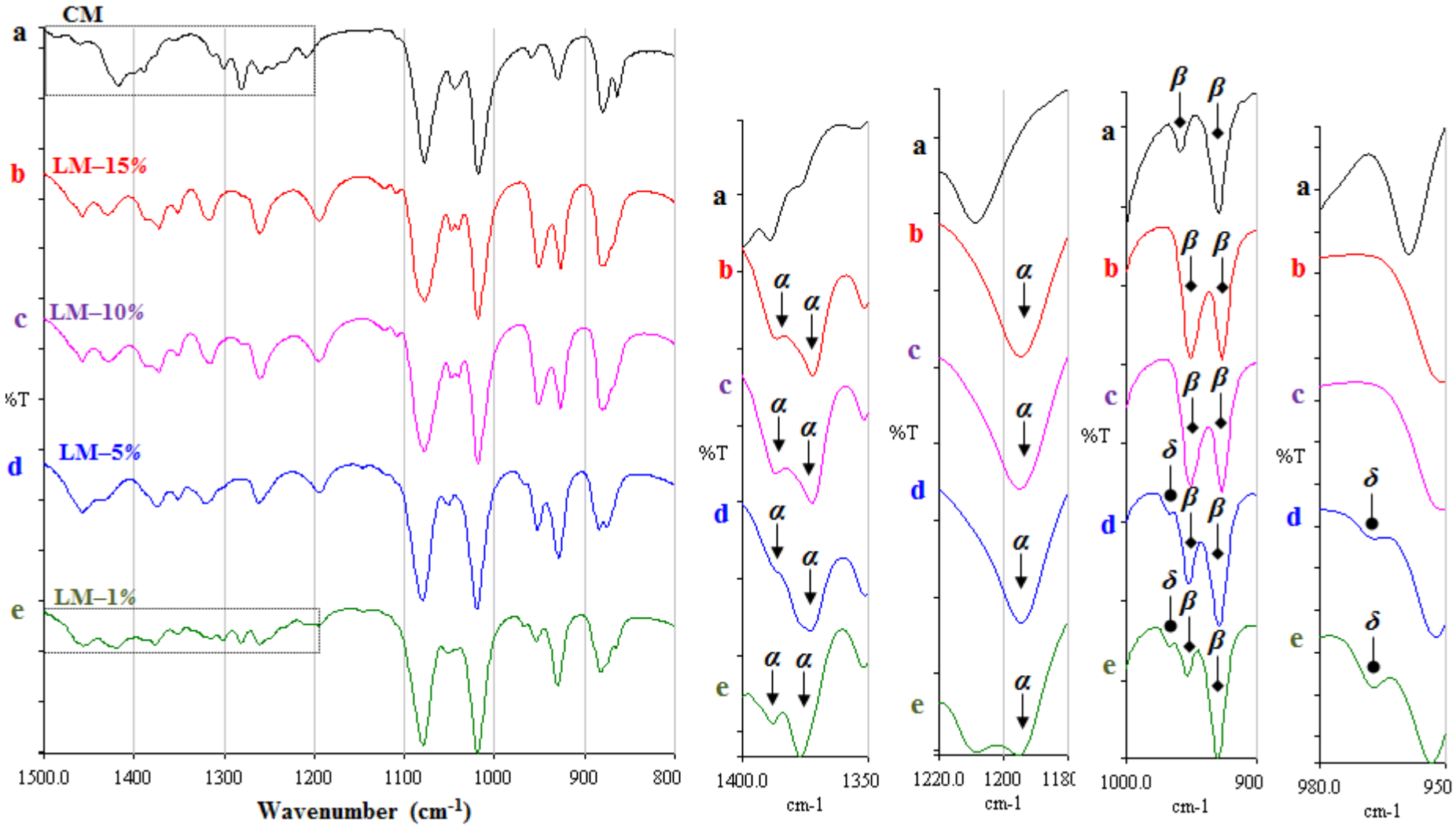

Figure 5. Fourier transform infrared spectroscopy (FT–IR) spectra of commercial mannitol (CM) (**a**) and mannitol lyophilised from a series of mannitol solutions with different concentrations, i.e., 15% (LM–15%) (**b**), 10% (LM–10%) (**c**), 5% (LM–5%) (**d**) and 1% *w*/*v* (LM–1%) (**e**) (%T: % transmittance).

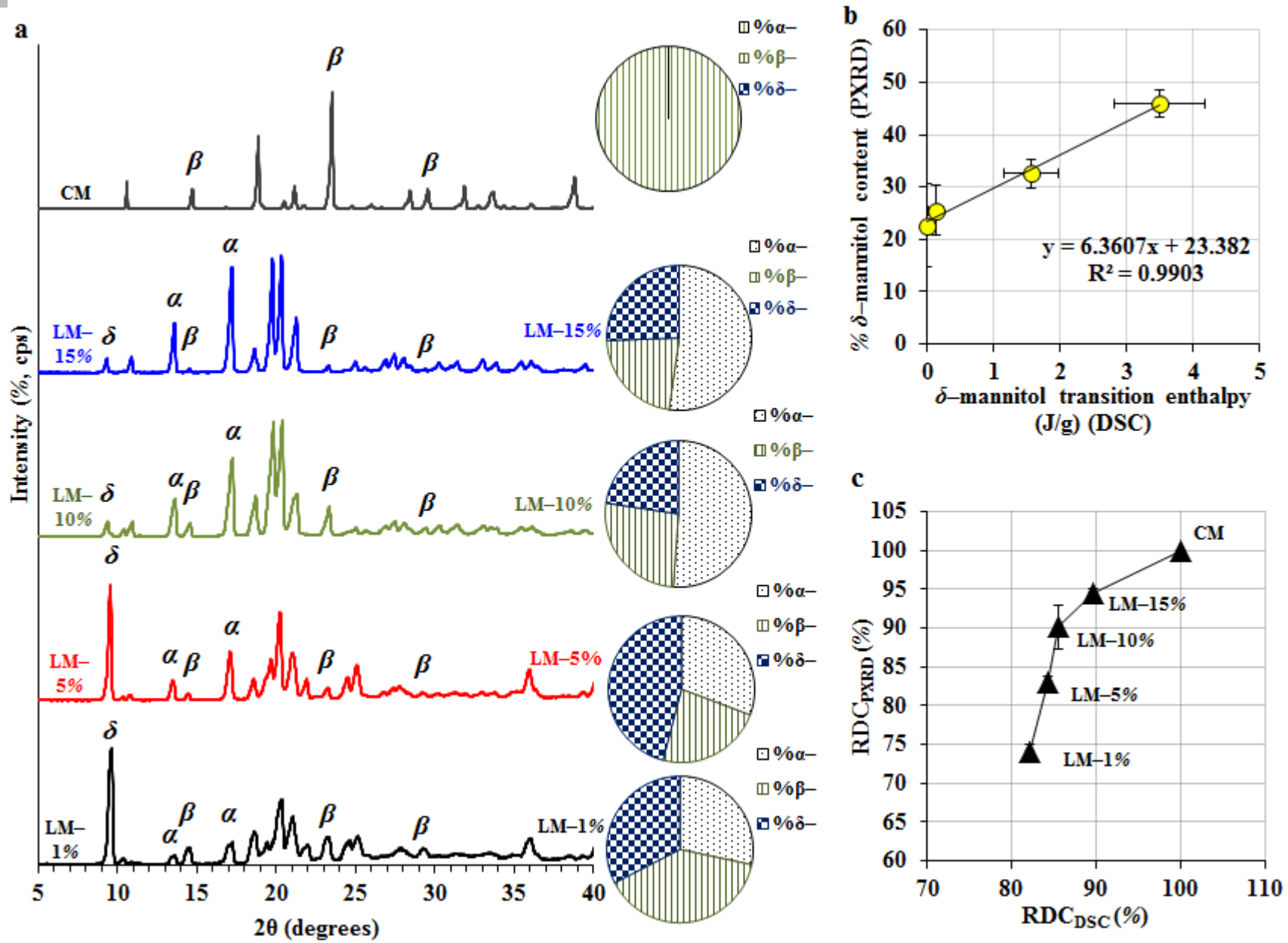

Figure 6. Powder X–ray diffraction (PXRD) patterns and % crystal form (mean ± SD, n = 4) (**a**); % δ–mannitol content estimated by PXRD relative to δ–mannitol transition enthalpy measured by DSC (**b**); and % relative degree of crystallinity estimated by PXRD (RDC_{PXRD}) relative to % relative degree of crystallinity estimated by DSC (RDC_{DSC}) (**c**) of commercial mannitol (CM) and mannitol lyophilised from a series of mannitol solutions with different concentrations, i.e., 15% (LM–15%), 10% (LM–10%), 5% (LM–5%) and 1% *w/v* (LM–1%).

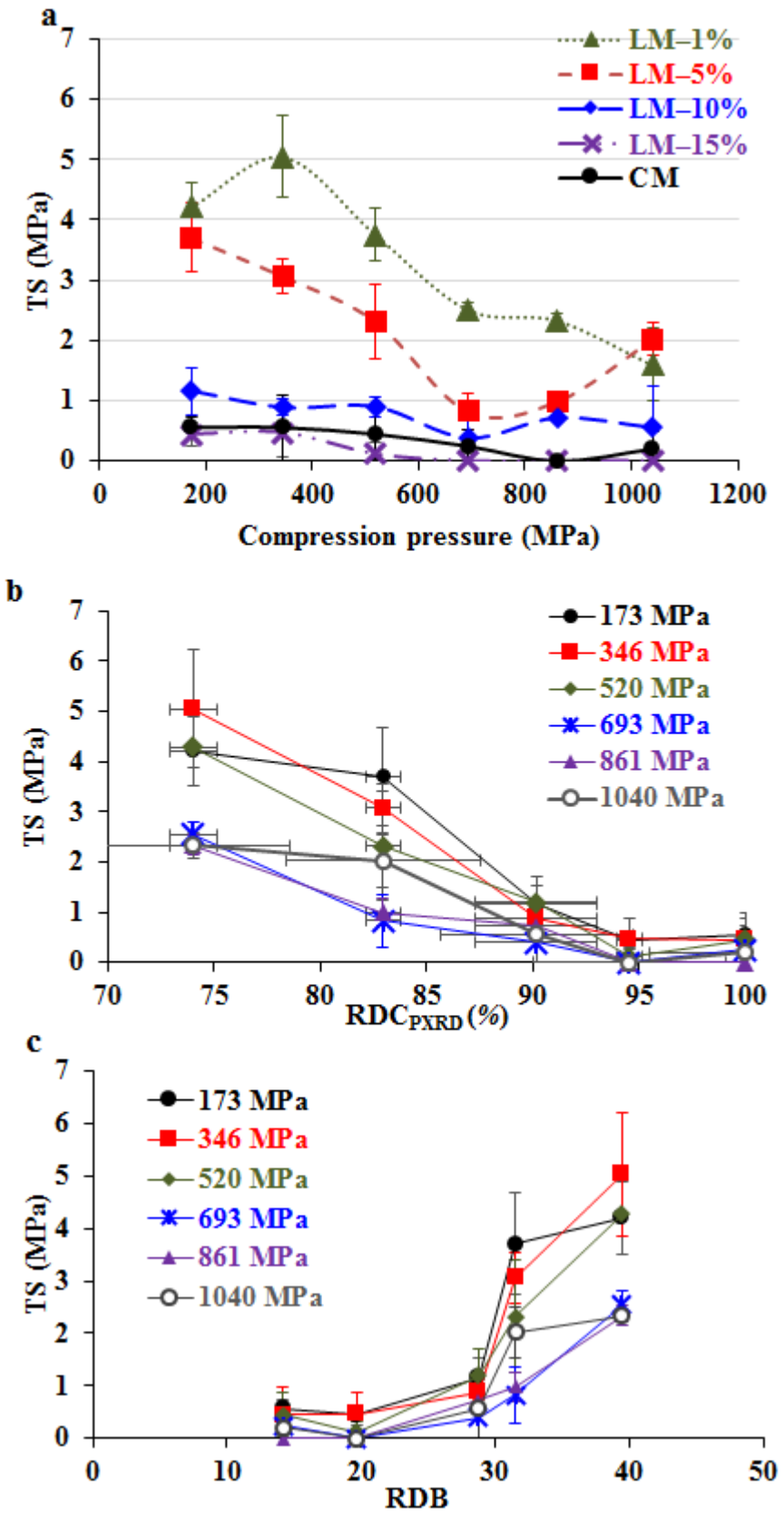

Figure 7. Tabletability profiles (mean ± SD, n = 5) of commercial mannitol (CM) and mannitol lyophilised from a series of mannitol solutions with different concentrations, i.e., 15% (LM–15%), 10% (LM–10%), 5% (LM–5%) and 1% *w*/*v* (LM–1%) (**a**); tensile strength (TS) of LM tablets compressed at different pressures (173 MPa to 1040 MPa) in relation to relative degree of crystallinity (RDC) (**b**) and relative degree of breakage (RDB) (**c**).

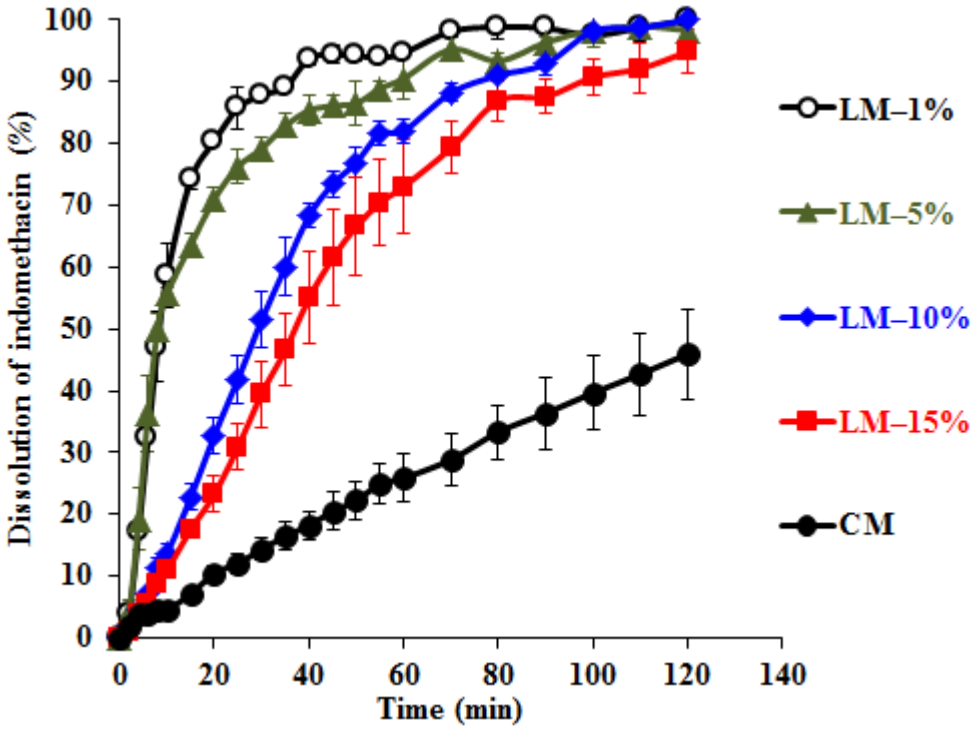

Figure 8. Dissolution profiles (mean ± SD, *n* = 3) for indomethacin tablets formulated with (●) commercial mannitol (CM) or mannitol lyophilised from a series of mannitol solutions with different concentrations, i.e., (■) 15% (LM–15%), (♦) 10% (LM–10%), (▲) 5% (LM–5%) and (○) 1% *w*/*v* (LM–1%).

Table 1. True density (D_{true}, mean ± SD, n = 9), bulk density (D_b), tap density (D_t), porosity, compactibility (1/a) (Eq. 3), cohesivity (1/b) (Eq. 3), and Carr's index (CI) (mean ± SD, n = 5) of commercial mannitol (CM) and mannitol lyophilised from a series of mannitol solutions with different concentrations, i.e., 15% (LM–15%), 10% (LM–10%), 5% (LM–5%) and 1% *w*/*v* (LM–1%).

Mannitol product	D_{true} (g/cm^3)	D_b (g/cm^3)	D_t (g/cm^3)	Porosity (%)	1/*a*	1/*b*	CI (%)	Flow character
CM	1.50 ± 0.02	0.45 ± 0.00	0.64 ± 0.04	65.0 ± 0.5	3.35 ± 0.45	3.58± 2.40	16.5 ± 0.8	Good
LM–15%	1.45 ± 0.02	0.11 ± 0.00	0.21 ± 0.01	91.1 ± 1.2	2.06 ± 0.03	9.74 ± 4.66	22.4 ± 2.3	Fair
LM–10%	1.39 ± 0.01	0.08 ± 0.00	0.15 ± 0.00	93.9 ± 0.8	2.14 ± 0.02	14.70 ± 4.43	28.7 ± 1.6	Poor
LM–5%	1.38 ± 0.04	0.05 ± 0.00	0.13 ± 0.02	95.7 ± 0.1	1.62 ± 0.20	15.28 ± 1.81	29.4 ± 1.1	Poor
LM–1%	1.22 ± 0.06	0.02 ± 0.00	0.06 ± 0.00	97.4 ± 0.4	1.49 ± 0.03	16.16 ± 1.71	37.1 ± 1.7	Very poor

Table 2. Particle size distribution (i.e. particle size at 10% ($d_{10\%}$), 50% ($d_{50\%}$, median diameter) and 90% ($d_{90\%}$) volume distribution and span) of commercial mannitol (CM) and mannitol lyophilised from a series of mannitol solutions with different concentrations, i.e., 15% (LM–15%), 10% (LM–10%), 5% (LM–5%) and 1% *w*/*v* (LM–1%).

Mannitol product	$d_{10\%}$ (µm)	$d_{50\%}$ (µm)	$d_{90\%}$ (µm)	Span
CM	61.6 ± 2.0	110.1 ± 3.0	177.6 ± 5.7	0.9 ± 0.1
LM–15%	8.9 ± 3.3	72.7 ± 11.2	196.5 ± 66.4	1.7 ± 0.0
LM–10%	18.1 ± 2.8	101.3 ± 2.2	259.7 ± 48.4	1.5 ± 0.1
LM–5%	23.0 ± 3.2	118.0 ± 4.8	269.6 ± 14.8	1.2 ± 0.0
LM–1%	48.6 ± 5.1	168.3 ± 5.5	288.1 ± 15.1	1.1 ± 0.0

Table 3. Dissolution efficiency (DE_{120min}), mean dissolution time (MDT), mean dissolution rate (MDR) of indomethacin, and amount of indomethacin (%) dissolved after 4 min (Q_{4min}), 10 min (Q_{10min}), 30 min (Q_{30min}) and 50 min (Q_{50min}) (mean ± SD, n = 3) from tablets containing commercial mannitol (CM) or mannitol lyophilised from a series of mannitol solutions with different concentrations, i.e., 15% (LM–15%), 10% (LM–10%), 5% (LM–5%) and 1% w/v (LM–1%).

Mannitol product	DE_{120min} (%)	MDT (min)	MDR (min^{-1})	Q_{4min} (min)	Q_{10min} (min)	Q_{30min} (min)	Q_{50min} (min)
CM	25.1 ± 6.3	54.1 ± 2.1	0.27 ± 0.07	4.0 ± 1.6	4.6 ± 1.2	14.4 ± 3.0	22.3 ± 5.3
LM–15%	62.7 ± 6.5	40.7 ± 6.9	0.70 ± 0.07	4.0 ± 1.0	10.9 ± 1.4	39.5 ± 9.3	66.6 ± 13.9
LM–10%	70.4 ± 1.3	35.5 ± 1.6	0.76 ± 0.07	4.7 ± 0.7	13.6 ± 1.4	51.5 ± 4.6	76.9 ± 2.5
LM–5%	83.4 ± 1.1	18.2 ± 0.3	1.19 ± 0.05	19.2 ± 5.0	55.7 ± 0.9	79.2 ± 1.8	86.5 ± 3.6
LM–1%	87.5 ± 0.4	15.0 ± 0.5	1.25 ± 0.07	17.1 ± 0.3	58.6 ± 5.1	87.8 ± 0.7	94.2 ± 0.9